SSC-435

PREDICTING STABLE FATIGUE CRACK PROPAGATION IN STIFFENED PANELS
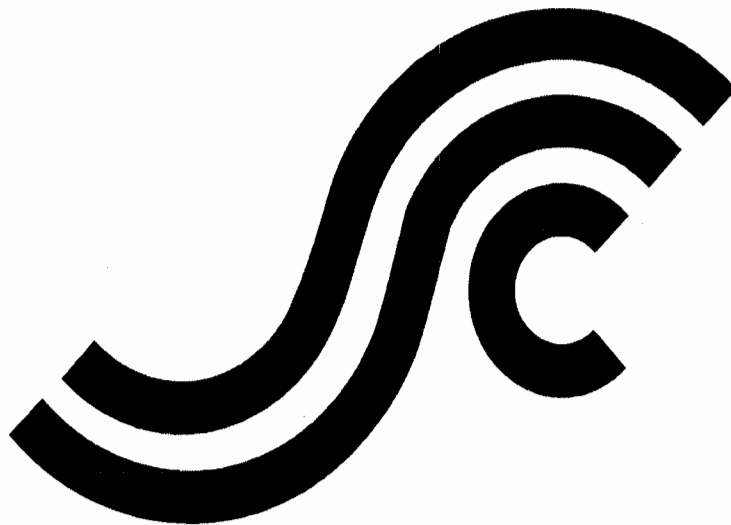
SHIP STRUCTURE COMMITTEE
2004

SHIP STRUCTURE COMMITTEE

RADM Thomas H. Gilmour
U. S. Coast Guard Assistant Commandant,
Marine Safety and Environmental Protection
Chairman, Ship Structure Committee

SSC – 435
SR – 1425

May 2004

PREDICTING STABLE FATIGUE CRACK PROPAGATION IN STIFFENED PANELS

This research builds upon research described in Ship Structure Committee report SSC-413, which had similar objectives and included fatigue experiments on stiffened panels incorporated in a highly redundant test fixture loaded in bending. This project conducted experiments in tension without redundancy or alternative load paths in the test fixture.

The models developed in this research are aimed at predicting the growth of large cracks after they become through-thickness cracks, and investigating the effect of residual stresses and redundancy on crack growth. A linear elastic fracture mechanics analysis was used to simulate crack propagation and gave reasonable agreement with the experiments.

The experiments and analyses, as in SSC-413, confirmed that crack propagation behavior can be conservatively predicted. The behavior in these experiments was not significantly different from those performed in the previous project in bending; indicating that the lack of bending stress gradient and redundancy did not alter the basic conclusion. The models developed in this project can be easily reproduced and can be used to assess the remaining life of ships with large cracks.

T. H. GILMOUR
Rear Admiral, U.S. Coast Guard
Chairman, Ship Structure Committee

Technical Report Documentation Page

1. Report No. SSC – 435	2. Government Accession Number	3. Recipient's Catalog No.
4. Title and Subtitle PREDICTING STABLE FATIGUE CRACK PROPAGATION IN STIFFENED PANELS		5. Report Date 31 March 2004
		6. Performing Organization Code
7. Author(s) Robert J. Dexter, and Hussam N. Mahmoud		8. Performing Organization Report No. SR-1425
9.Performing Organization Name and Address University of Minnesota Department of Civil Engineering 122 CivE, 500 Pillsbury Dr. S.E. Minneapolis, MN 55455-0116		10. Work Unit No. (TRAIS)
		11. Contract or Grant No. DTCG32-01-F-100015
12. Sponsoring Organization Name and Address Ship Structure Committee U. S. Coast Guard (G-MSE/SSC) 2100 Second Street, SW Washington, D.C. 20593-0001		13. Type of Report & Period Covered Final Report
		14. Sponsoring Agency Code G-M

15. Supplementary Notes

Sponsored by the Ship Structure Committee. Jointly funded by its member agencies.

16. Abstract (MAXIMUM 200 WORDS)

Fatigue tests in cyclic tension were conducted on approximately half-scale welded stiffened panels to study propagation of large cracks as they interact with the stiffeners. A linear elastic fracture mechanics analysis was used to simulate the crack propagation and gave reasonable agreement with the experiments. The range in stress intensity factor (ΔK) was determined with either a finite-element analysis or an analytical model at increments of crack length. Models included an idealized residual stress distribution similar to measured residual stresses. Crack propagation rate as a function of ΔK was estimated using the Paris law with upper-bound coefficients. The predicted growth rate was most sensitive to the residual stress and the Paris law coefficient. The experiments and analyses show little sensitivity to stiffener type. The models developed in this project can be easily reproduced and can be used to assess the remaining life of ships with large cracks, leading to more accurate assessment of safety and more efficient scheduling of repairs.

17. Key Words Ship, Fatigue, Residual stresses, Long cracks, Weld	18. Distribution Statement Distribution unlimited, available from: National Technical Information Service Springfield, VA 22161 (703) 487-4650

19. Security Class (This Report) UNCLASSIFIED	20. Security Class (This Page) UNCLASSIFIED	21. No of Pages	22. Price

CONVERSION FACTORS
(Approximate conversions to metric measures)

To convert from	to	Function	Value
LENGTH			
inches	meters	divide	39.3701
inches	millimeters	multiply by	25.4000
feet	meters	divide by	3.2808
VOLUME			
cubic feet	cubic meters	divide by	35.3149
cubic inches	cubic meters	divide by	61,024
SECTION MODULUS			
inches^2 feet^2	centimeters^2 meters^2	multiply by	1.9665
inches^2 feet^2	centimeters^3	multiply by	196.6448
inches^4	centimeters^3	multiply by	16.3871
MOMENT OF INERTIA			
inches^2 feet^2	centimeters^2 meters	divide by	1.6684
inches^2 feet^2	centimeters^4	multiply by	5993.73
inches^4	centimeters^4	multiply by	41.623
FORCE OR MASS			
long tons	tonne	multiply by	1.0160
long tons	kilograms	multiply by	1016.047
pounds	tonnes	divide by	2204.62
pounds	kilograms	divide by	2.2046
pounds	Newtons	multiply by	4.4482
PRESSURE OR STRESS			
pounds/inch^2	Newtons/meter^2 (Pascals)	multiply by	6894.757
kilo pounds/inch^2	mega Newtons/meter^2 (mega Pascals)	multiply by	6.8947
BENDING OR TORQUE			
foot tons	meter tons	divide by	3.2291
foot pounds	kilogram meters	divide by	7.23285
foot pounds	Newton meters	multiply by	1.35582
ENERGY			
foot pounds	Joules	multiply by	1.355826
STRESS INTENSITY			
kilo pound/inch^2 inch$^{\frac{1}{2}}$(ksi$\sqrt{}$in)	mega Newton MNm$^{3/2}$	multiply by	1.0998
J-INTEGRAL			
kilo pound/inch	Joules/mm^2	multiply by	0.1753
kilo pound/inch	kilo Joules/m^2	multiply by	175.3

ACKNOWLEDGMENT

TABLE OF CONTENTS

LIST OF TABLES

LIST OF FIGURES

EXECUTIVE SUMMARY

Fatigue cracks may propagate in ship hull structure in a stable manner with a length exceeding the stiffener spacing. The numbers of cycles of stable propagation can be substantial; on the order of double the number of cycles to develop a through-thickness crack, the traditional definition of "failure" or end of the fatigue life. The ability to confidently predict this additional life would increase confidence in safety assessments of ships with known fatigue cracks and allow more efficient scheduling of repairs. Therefore, this research was conducted at the University of Minnesota to develop models aimed at predicting the growth of cracks after they become through-thickness cracks.

This research builds upon research described in Ship Structure Committee report SSC-413. This previous project had similar objectives and included fatigue experiments on stiffened panels incorporated in a highly redundant test fixture loaded in bending. In the present work, the experiments were conducted in tension without redundancy or alternative load paths in the test fixture. Five such experiments were conducted on specimens consisting of plates about 3450 mm long and 1625 mm wide with four welded longitudinal stiffeners. A through-thickness crack was started at the middle of the plate and this crack propagated transversely in both directions through each of the stiffeners under a constant-amplitude cyclic tension load. The crack length was recorded versus number of cycles.

The experimental results were modeled using linear-elastic fracture mechanics analysis. The range in stress intensity factor (ΔK) was determined with either a finite-element model or an analytical model at increments of crack length. Both models included the same idealized residual stress distribution, which was similar to measured residual stresses. Both approaches can be used and they were in reasonable agreement with each other. Crack propagation rate as a function of ΔK was estimated using the Paris law with published upper-bound coefficients for structural steel. The predicted growth rate was most sensitive to the magnitude of the residual stress and the Paris law coefficient. The experiments and analyses show little sensitivity to stiffener type.

As in the previous project, these experiments and analyses confirmed that this stable crack propagation behavior can be relied upon and can be conservatively predicted. The behavior in these experiments was not significantly different from those performed in the previous project in bending; indicating that the lack of bending stress gradient and redundancy did not alter this basic conclusion. The models developed in this project can be easily reproduced and can be used to assess the remaining life of ships with large cracks.

1   INTRODUCTION

1.1   Problem Statement

Generally, crack-like discontinuities or flaws exist in the structural elements due to welding. Under cyclic loading, a flaw can develop into a fatigue crack and propagate until fracture occurs. Fracture mechanics is used to analyze and predict the behavior of a cracked structural element.

Ships are very redundant and cracks are usually not an immediate threat to the integrity of the ship. However, fatigue cracks could grow to be as large as 24 meters as shown in Figure 1-1. These long cracks remain surprisingly stable because of minimum notch-toughness levels specified for ship steel and the redundancy. However, even if brittle fracture does not occur, at some point a net-section plastic collapse of the structure will occur, leading to a failure of the entire ship.

Figure 1-1 Cracked deck in the tanker Castor [1]

Fracture toughness and ductility of the structural steel are important for redundancy to be effective. In a steel member, the capacity of the member decreases as the crack propagates farther in the member. However, if the member has sufficient fracture toughness, it can tolerate a crack so large that the applied load exceeds the capacity for the net section causing plastic deformation to occur in the member. The plastic deformation allows the load to be shed to other members. However, net-section yielding is not very ductile unless the yielding can spread to the gross section, which requires strain hardening in the stress-strain relationship of the steel, or a reasonably low yield-to-tensile ratio [2].

A large tanker may have hundreds or even thousands of fatigue cracks discovered during inspection. These cracks are usually not an immediate threat to the structural integrity of the ship. Guidelines prepared by Tanker Structure Co-operative Forum are used for the inspection and maintenance of tanker structure [3, 4]. The tolerance of ships to these cracks is a function of the overall structural redundancy and ductility, as well as fracture toughness of the structural components.

The S-N curve approach is the most common method used for determining the fatigue life of a structural detail. The S-N curve is a lower bound to fatigue test data in terms of the stress range (S) and number of cycles to failure (N). Failure in the tests is usually defined as the development of through-thickness cracks (typically about 100 mm in length).

Although the 24 m crack shown in Figure 1 is an extreme case, it is not unusual to find cracks several meters long in a ship. The additional life for a through-thickness crack about 100 mm in length to grow to a length of several meters is quite substantial. Furthermore, if a high level of redundancy, ductility, and fracture toughness exist in the structure, the growth could be stable giving additional time to more efficiently schedule repair and maintenance.

1.2 Research Objective

Several studies on cracks in riveted aircraft stiffened panels have been conducted. However, few studies on crack growth in panels with welded stiffeners have been performed. Furthermore, no studies on crack growth in plates with welded stiffeners have been conducted where the panels are loaded axially. Welded stiffeners affect crack growth because of residual stresses present from the welding process. The high heat input from the welding process causes high tensile stresses in the vicinity of the stiffeners. The tensile stresses are equilibrated by compressive stresses in the region between the stiffeners. These residual stresses decrease the crack growth rate between stiffeners. Depending on the magnitude of the compressive residual stresses and the stress ranges, the crack growth can even arrest completely.

Previous studies were done on box sections with edge webs and/or multiple stiffeners. The results showed stable propagation of the crack. It was believed that a main factor in the stability of the growth was redundancy. Therefore, testing a single plate with no redundancy was essential in quantifying the effect of redundancy on the crack growth rate.

Unfortunately, because of the large loading demand, very limited research on stiffened panels has been performed in the past where the panel was to be loaded axially. Dexter and Pilarski conducted recent related research [5, 6]. In this previous research, stiffened panels were loaded in four-point bending to reduce the necessary load. However, putting the specimen under bending created a stress gradient through the thickness. This bending gradient resulted in zero stress somewhere along the stiffener's web at the location of the neutral axis, and caused the end of the crack propagating up the stiffener to arrest.

The models developed in this research are aimed at predicting the growth of large cracks after they become through-thickness cracks, and investigating the effect of residual stresses and redundancy on crack growth.

2 BACKGROUND

The reader is advised to refer to the Ship Structure Committee report SSC 413 by Dexter and Pilarski [6], which provides an extensive literature review for the background on the subject of fracture mechanics as well as fatigue crack propagation in welded stiffened panels. Some of the background is presented here.

2.1 Introduction to Fracture Mechanics

The theory of fracture mechanics can be used to predict fracture as well as fatigue crack propagation. For the purpose of predicting fatigue crack propagation, the plasticity at the crack tip is limited and therefore Linear Elastic Fracture Mechanics (LEFM) is adequate. Fracture mechanics problems can be described in terms of three modes of loading, mode I, II, and III as illustrated in Figure 2-1.

Mode I, also known as the opening mode, is the case where the crack faces are moving apart when the load is acting perpendicular to the crack plane. Mode II is called the sliding mode (in-plane shear). Mode III is called the tearing mode. Fatigue crack propagation is usually Mode I, so this will be the focus in this report.
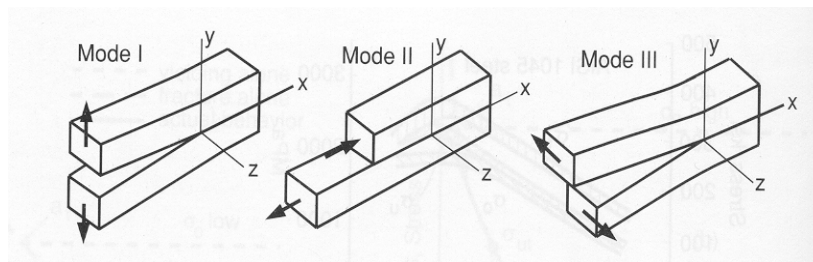
Figure 2-1 The three modes of loading

2.2 Linear Elastic Fracture Mechanics

LEFM is based on a parameter called the stress-intensity factor (K), which can be considered a measure of the magnitude of the crack tip stress and strain fields. This parameter is related to the applied stress and crack size by the formula:

$$K = F_c \, F_s \, F_w \, F_g \; \sigma(\pi a)^{1/2} \qquad\qquad \textit{Equation 2.2-1}$$

Where: F_c = crack shape factor

F_s = crack surface factor (F_s = 1.12 if the crack originates at a surface)

F_w = finite width factor

F_g = non-uniform stress factor

a = half the crack length

The stress intensity factor has units of MPa-m$^{1/2}$ or ksi-in$^{1/2}$. A given material can resist a crack without brittle fracture as long as K is below a critical value K_c, (i.e. K<K_c) [7, 8]. The value of K_c is the fracture toughness of a material. Temperature, loading rate, and material thickness are parameters that affect the material toughness.

2.3 Strain Energy Release rate

For a crack growing in mode I, the energy release rate "G" is defined in Figure 2-2 as a function of the material thickness (t) and the change in energy (dU) to extend the crack a distance (da). The crack will extend when the energy available to grow the crack is high enough to overcome the resistance provided by the material [8]. Figure 2-2 (a) describes the energy stored in the material as it is loaded with force P. When the crack extends a distance da, the stored energy (U) in the body is released and consumed to form the new crack of length (a + da). The stored energy is decreased by an amount (dU), and the total stored energy in the body becomes (U − dU). The value of (G) could be measured experimentally. However, the stress intensity factor is a more preferred term to use in linear elastic fracture mechanics. The quantities G and K are related by the formula:

$$G = \frac{K^2}{E} \quad (\text{plane stress; } \sigma_z = 0) \qquad\qquad \textit{Equation 2.3-1}$$

(a)

(b)

$G = (-1 / t) x (du / da)$
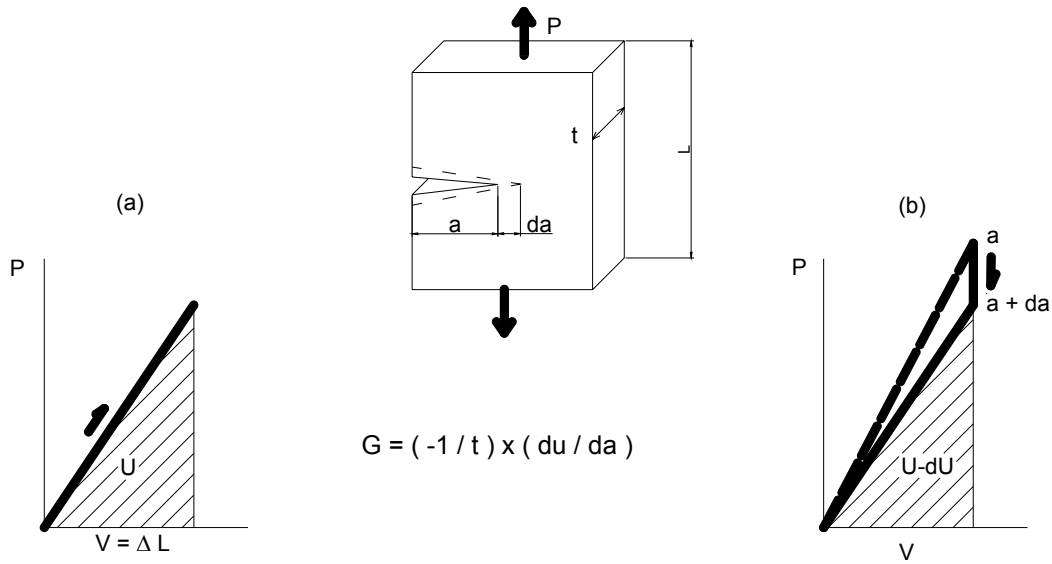
Figure 2-2 Potential energy for a crack of length a and a crack da (adapted from [8])

2.4   The Stress Intensity Factor K

The stress intensity factor K characterizes the intensity of the stress surrounding a sharp crack tip in a linear elastic and isotropic material [8]. Around a sharp crack tip, the stresses are defined by equations 2.4-1, which describe the stresses in the vicinity of a crack as shown in Figure 2-3. Applying Equation 2.4-1, one could see that at the crack tip the stresses approach infinity causing singularity (i.e. unknown stresses).

$$\sigma_x = \frac{K_I}{\sqrt{2\pi r}}\cos\frac{\theta}{2}\left[1-\sin\frac{\theta}{2}\sin\frac{3\theta}{2}\right]+.......... \qquad \text{(a)}$$

$$\sigma_y = \frac{K_I}{\sqrt{2\pi r}}\cos\frac{\theta}{2}\left[1+\sin\frac{\theta}{2}\sin\frac{3\theta}{2}\right]+.......... \qquad \text{(b)}$$

$$\tau_{xy} = \frac{K_I}{\sqrt{2\pi r}}\cos\frac{\theta}{2}\sin\frac{\theta}{2}\cos\frac{3\theta}{2}+.......... \qquad \text{(c)} \quad \textit{Equations 2.4-1}$$

$$\sigma_z = 0 \qquad\qquad\qquad \text{for plane stess} \qquad \text{(d)}$$

$$\sigma_z = \upsilon(\sigma_x + \sigma_y) \qquad\qquad \text{for plane strain} \qquad \text{(e)}$$

$$\tau_{yz} = 0 \,(\text{f})$$
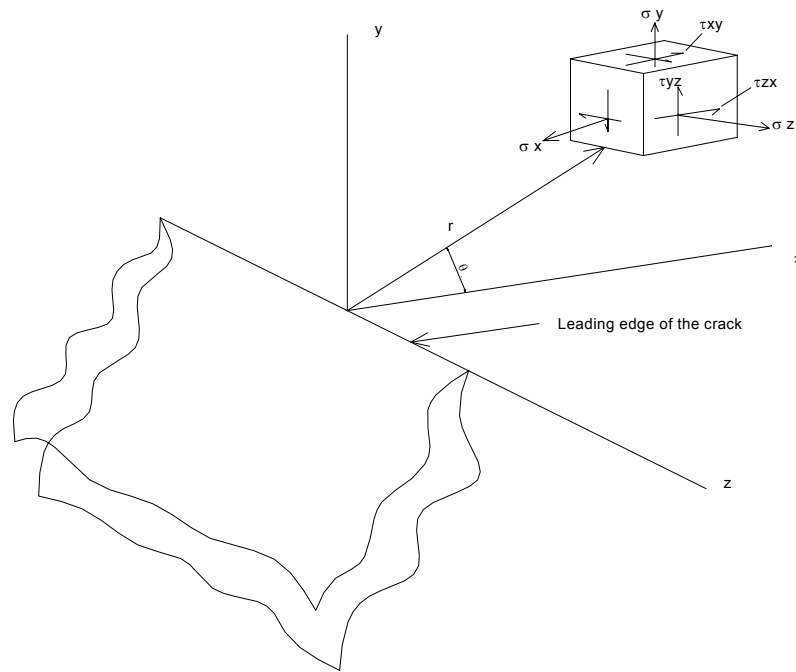
Figure 2-3 Three-dimensional coordinate system for a region of a crack tip (adapted from [8])

In a mathematical sense, K_I at the crack tip is defined as follows:

$$K_I = \lim_{r,\theta\to 0}(\sigma_y\sqrt{2\pi r}) \qquad\qquad \textit{Equation 2.4-2}$$

Equation 2.4-2 could also be written as:

$$K = Y\sigma\sqrt{\pi a}$$

Equation 2.4-3

Where: σ = applied nominal gross-section tensile stress (see Figure 2-4)

a = half the crack length

Y = the product of all correction factors in equation 2.2-1
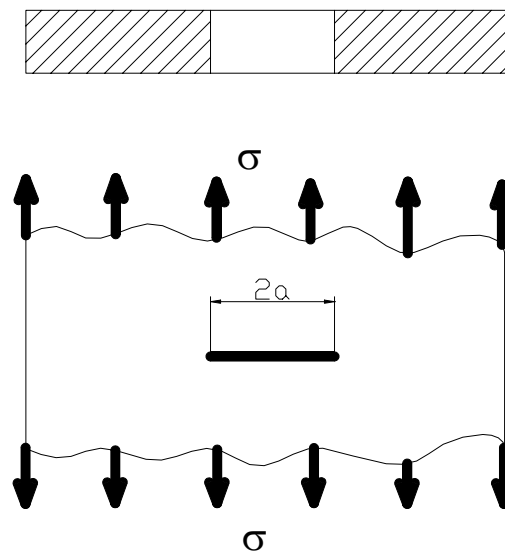
Figure 2-4 Through thickness crack in an infinite plate under tension

2.5 Modeling of Fatigue Crack Growth

The rate of change of crack length (a) with number of cycles (N) in fatigue crack growth can be described using a model having the general form of Equation 2.5-1.

$$da/dN = f(\Delta K, R)$$

Equation 2.5-1

Where R is the load ratio or the ratio of minimum load to maximum load. Rushton [9] describes various models that were developed and used to predict fatigue crack growth. Most of the models have the form of a power law, which is associated with curve fitting

8

parameters that do not have a physical significance. One of the most reliable and effective models used for predicting fatigue crack growth is the Paris model, also known as the Paris Law.

2.6 The Paris Law

Paris and Erdogan [10] hypothesized in 1963 that the range in stress-intensity factor, ΔK, governs fatigue crack growth. The empirical Paris Law represents the crack growth rate data as a straight line when plotted on a log-log scale [10]. However, experimental da/dN verses ΔK data typically exhibit a sigmoid shape when plotted on a log-log scale. There is a ΔK threshold, ΔK_{th}, below which cracks will not propagate. ΔK_{th} can be taken as 3 MPa-m$^{1/2}$ for structural steel. The Paris Law is fit to the linear portion of the da/dN versus ΔK plot (on a log-log scale) that lies above ΔK_{th}. At relatively high ΔK levels the crack growth rate accelerates, and is accompanied by ductile tearing or increments of brittle fracture in each cycle.

The Paris Law is expressed as:

$$\frac{da}{dN} = C * (\Delta K)^m \qquad\qquad \textit{Equation 2.6-1}$$

Where: a = half the crack length

N = number of cycles

C = an experimentally determined coefficient

ΔK = stress intensity factor range

m = material constant

It is difficult to achieve great accuracy in predicting crack growth rate when using fracture mechanics [11]. There is up to a factor of twenty in the scatter of experimental da/dN data. A great deal of the scatter is due to experimental error, especially at low growth rates near the threshold. In this range, the growth rate is affected by the

procedure used to pre-crack the specimens at higher ΔK. There is a great deal of inherent variability in the actual growth rates, even if they were to be accurately measured.

The value of m, the exponent in the Paris Law, is typically taken as 3.0 for steel. The relation between the Paris Law describing the stress intensity factor for a specific crack length and the S-N curve is such that the exponent is the same as the inverse slope of the S-N curves when plotted on a log-log scale.

Crack growth rate depends on the load ratio (R) as indicated in Equation 2.5-1. Different lines may be fit to the experimental data (on a log-log plot) for different load ratios. There are also empirical equations that account for the effect of the load ratio on the crack growth rate. The preferred approach is to account for the effect of load ratio and associated crack closure in the definition of ΔK. The idea is that the baseline crack growth rate model is defined for high load ratios (greater than 0.7), for which there is negligible crack closure. At lower load ratios (less than 0.5) and negative load ratios the crack is closed for part of the load cycle, and only the part of the load cycle where the crack is open is effective. An effective ΔK_{eff} is defined as that part of ΔK that contributes to the crack propagation, and then ΔK_{eff} is used in Equation 2.6-1, where the parameters of Equation 2.6-1 are defined by fitting the equation to high R crack growth rate data. This is the approach taken in this research, and the Paris Law will be assumed to be defined for high load ratio (greater than 0.7). Crack closure is discussed in greater detail in Section 2.9.

Variance in the crack growth rate is usually expressed by variance in the coefficient C. Most researchers agree that all C-Mn steels have similar crack growth rates, and that the variance observed is just the typical material variation. In other words, there is no significant difference in the crack growth rates among various types of C-Mn steel, there is only scatter. Therefore, most reported values of C are intended to represent a conservative upper bound to the data.

Barsom and Rolfe [12] established an upper bound for a variety of ferritic steels where C was 6.8 x 10^{-12} for units of MPa and meters. The Barsom and Rolfe relation seems to be unconservative for high-load-ratio crack growth rates, however. Fisher, et al. [14] performed a study of HSLA-80 steel, which showed that the upper bound value of C for high-load-ratio data was 9.0 x 10^{-12}. British Standards Institute BS 7910 [13] recommends an upper bound of 16.5 x 10^{-12} for C. However, this value seems to be excessively conservative. In a previous version of this document known as PD 6493, a more reasonable upper bound of 9.5 x 10^{-12} was recommended for C. Table 2-1 shows different values of the constant C from various sources.

Table 2-1 Values of C present in different sources

Reference of C values	C MPa and m
Barsom and Rolfe [12]	6.8 x 10^{-12}
Fisher et.al. [14]	9.0 x 10^{-12}
BS 7910 [13]	16.5 x 10^{-12}
BSI PD 6493 [15]	9.5 x 10^{-12}

2.7 Crack Propagation in Stiffened Panel

There has been extensive previous research on the solution for the stress intensity factor for a crack propagating in a stiffened panel. The majority of the work was done to investigate the growth of a crack in an aluminum panel for application to the aviation industry. Poe [16] proposed a numerical solution for K in a cracked panel with uniformly spaced riveted stiffeners. Poe introduced a parameter called "percent stiffening", which compares the area of the stiffeners to the total area of the stiffeners and the plate. He introduced this ratio and defined it as μ. That is:

$$\mu = \frac{A_{st}E_{st}}{AE + A_{st}E_{st}}$$

Equation 2.7-1

Where: A_{st} = area of the stiffeners

   A = area of the plate

   E_{st} = Young's Modulus of the stiffeners

   E = Young's Modulus of the plate

Poe [17] developed a solution for a crack propagating in a stiffened plate where the stiffeners were attached to the plate by means of rivets, and noticed that the K solution decreases as the crack approaches a stiffener, indicating that the stiffener aided in restraining the crack or slowing down the propagation. Poe also realized that the riveted stiffeners continue to limit crack growth after the crack propagates past the stiffener since a crack cannot propagate directly up into the stiffener.

However, in a welded stiffener the crack may propagate into and completely sever the stiffener. For integral stiffeners such as welded stiffeners, Poe developed a solution that assumed that once a crack reaches a stiffener, the stiffener is completely and suddenly severed and the load previously carried by the stiffener is shed to the remaining net section. Figure 2-5 depicts this solution, which shows the jump in the K value as a result of the stiffener being immediately severed.

Poe also did an experiment on panels with integral stiffeners where the integrally stiffened panels were made from an aluminum sheet extruded without standing stiffeners. In the actual experiment, Poe noticed that the crack propagated in the stiffener with the same rate it propagated in the plate. Therefore, he proposed a linear increase in the stress intensity factor between the value for an intact stiffener and the completely severed stiffener at a point where the distance beyond the stiffener was equal to the height of the stiffener.
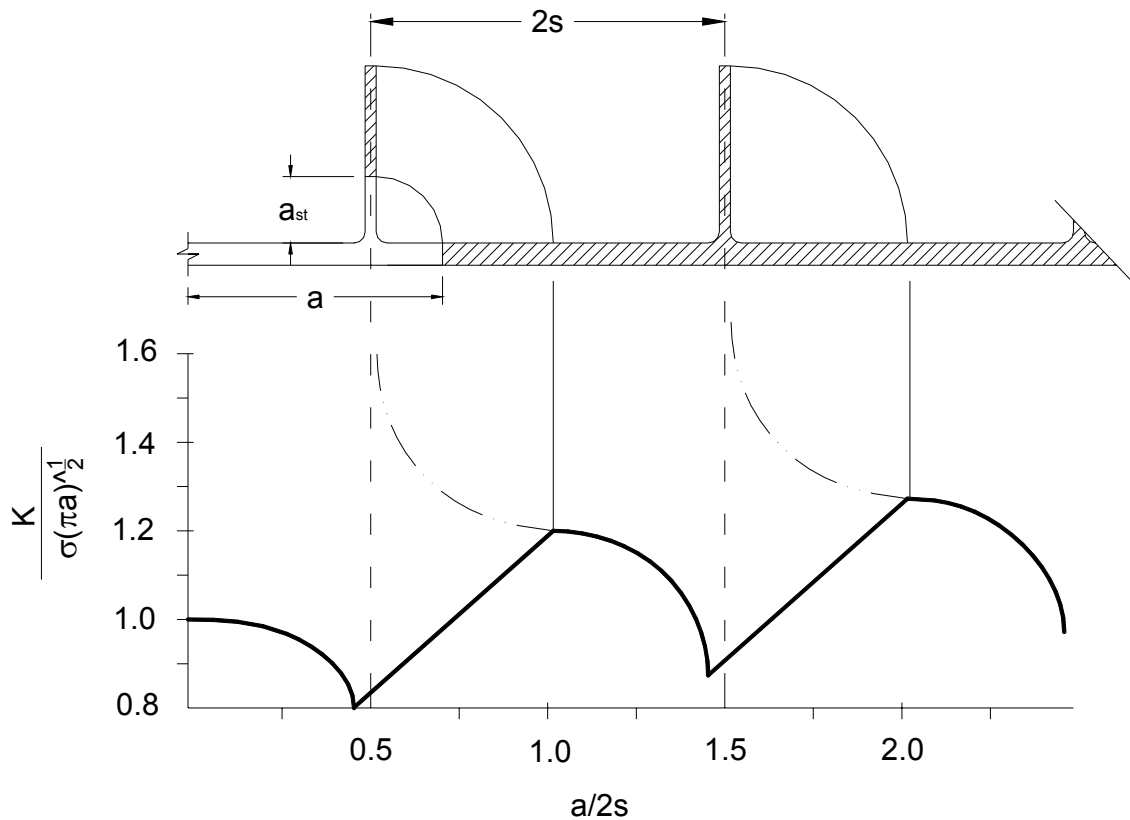
Figure 2-5 K solution for a panel with integral stiffeners

Because there are only localized residual stresses induced in a plate with riveted connections and integrated stiffeners by extrusion, the study did not include the effect of residual stresses. The K value obtained from Poe's model along with the Paris Law for crack propagation became a solid foundation for crack propagation in aircraft panels.

Thayamballi [18] studied the effect of residual stresses on crack propagation in welded stiffened panels, and outlined an analytical approach to calculate the fatigue crack growth. The contribution of the residual stresses to K was based on Greene's function, integrating the solution for a pair of forces acting on the crack faces. A block tension and compression region, which was suggested by Faulkner [19], was used for the residual stress distribution.

Petershagen and Fricke [20] conducted several fatigue crack growth experiments on welded stiffened panels with cutouts. They reported that the influence of welded stiffeners on the propagation of the crack was rather small, and that at least for the test condition in their experiments, residual stresses did not seem to effect the propagation of the crack!

Using a three-flanged box beam to simulate the structural redundancy found in a doubled-hulled ship structure, Nussbaumer [21] performed a study on crack propagation in large-scale experiments on welded box girders. He also investigated the effect of residual stresses on the propagation of the crack using finite element analysis and applying fictitious temperature fields to give thermal stresses in reasonable agreement with the initial residual stresses measured in the box girder.

There was significant scatter in the measured residual stress distributions for these box girders. Therefore, three distributions were examined for the finite-element modeling based on the smallest, largest, and average observed residual stresses measured in the specimen. Nussbaumer showed that the results were quite sensitive to the magnitude of residual stresses used for the analysis. A similar approach was followed in this project as discussed in Chapter 4, resulting in comparable observations.

In Nussbaumer's study, many other variables, including the difference between the upper bound growth rate and the lower bound growth rate, made minimal difference in the calculations in comparison to the residual stress. He concluded that more effort should be put into studying residual stress and how it is affected by fabrication sequence.

Dexter and Pilarski [5, 6] further extended Nussbaumer's work to the case of multiple stiffener plate geometry rather than the un-stiffened cellular geometry. They tested box sections with drain holes, raised drain holes, and weld access holes. As shown in Figure 2-6, the box sections were tested in four-point bending to create a region of constant bending moment and monitor crack propagation throughout that region.
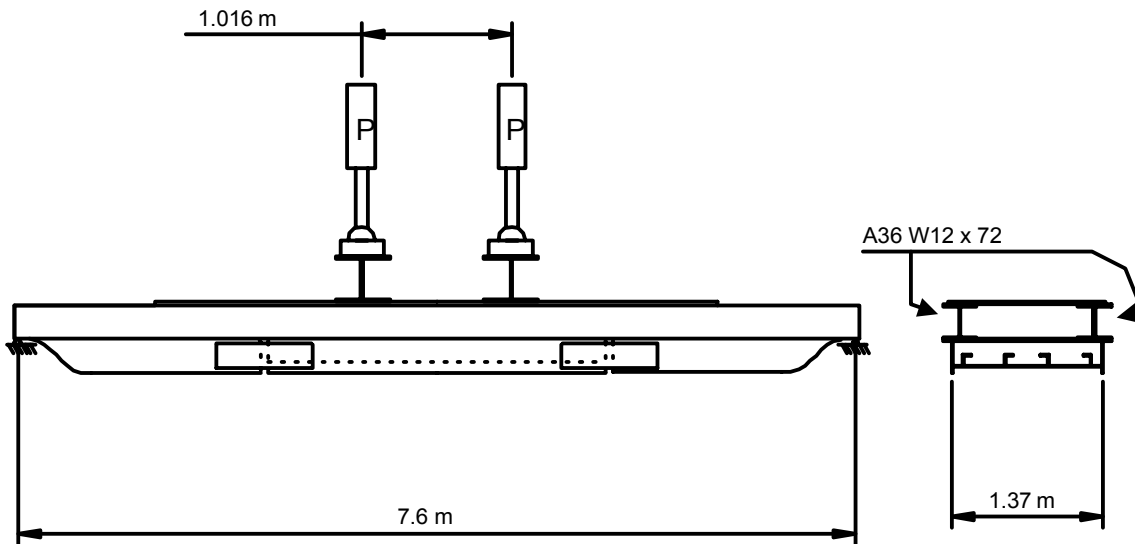
Figure 2-6 Test setup used by Dexter and Pilarski

They found that the redundancy in the box sections helped to stabilize crack propagation in the stiffeners, allowing the crack to exceed 1500 mm in length in some cases.

2.8   Residual Stresses

Two types of residual stresses exist in a ship structure. The first are mechanical stresses, which are introduced through construction sequencing (i.e. internal stresses that result from improper fit and assembly distortion). A ship structure can be regarded as an assemblage of continuous stiffened plates with equally spaced longitudinal stiffeners of approximately the same size [22]. For a proper fit of these stiffened plates, it is not unusual to mechanically force the plates or the structural components into certain positions. Forcing these components in place along with the applied weld could easily result in locked-in stresses.

There is an intimate relationship between mechanical residual stress and welding-induced residual stress, the first often affected by welding distortion. Welding residual stress arises from heat introduced by the welding processes. The heat input used for the

welding process as well as the sequence at which the stiffeners are welded to the plates can have a great influence on the distribution of residual stresses in the plate, affecting the crack propagation. This is discussed further in section 3.5.2 .

As mentioned previously, residual stresses are considered one of the main factors affecting the propagation of a crack under fatigue cycles. Therefore, an understanding of the magnitude and the distribution of these stresses is important in studying the crack propagation behavior. Early work on measuring residual stresses was done by Heyn and Bauer, and dates back to 1911. They measured residual stresses in bars and rods by relating the change in length of the rod to the existing residual stresses in the specimen.

Osgood [23] investigated the effect of residual stresses on crack propagation in ship hulls. Fitzpatrick and Edwards [24] provided a good overview of the effect of residual stresses on predicting fatigue crack growth.

There are various methods for measuring residual stresses. J. Lu [25] provided a good handbook on the different measuring techniques practiced by engineers and researchers. The scatter and the inherent variability make it difficult to have an accurate assessment of the actual distribution and/or magnitude of the residual stresses existing in a structural component.

High tensile residual stresses exist in the vicinity of the stiffener-to-plate welds, while compressive residual stresses exist between the stiffeners. The uncertainty in the additional life due to long crack propagation is dominated by the uncertainty in the magnitude of the compressive residual stress. Variations in the expected residual stresses are due to the initial residual stresses in the plates and rolled shapes prior to welding, thermal cutting, and fabrication. The resulting uncertainty can change the crack propagation rate by more than two orders of magnitude.

In this project, Faulkner's model for residual stress distribution [19] was used to represent the distribution of the stresses, and was then incorporated in the finite element model as a simple representation of the actual residual stress present in the stiffened panels. Figure 2-7 shows Faulkner's model with the tensile regions around the stiffeners represented as a tension block having a base width proportional to the plate thickness (η x t $_{plate}$) where the value of η typically ranges between 3.5 and 4 in a ship structure after shakedown. The tensile region resulting from the welding process is balanced by a compression region, which is very beneficial in slowing down the crack.
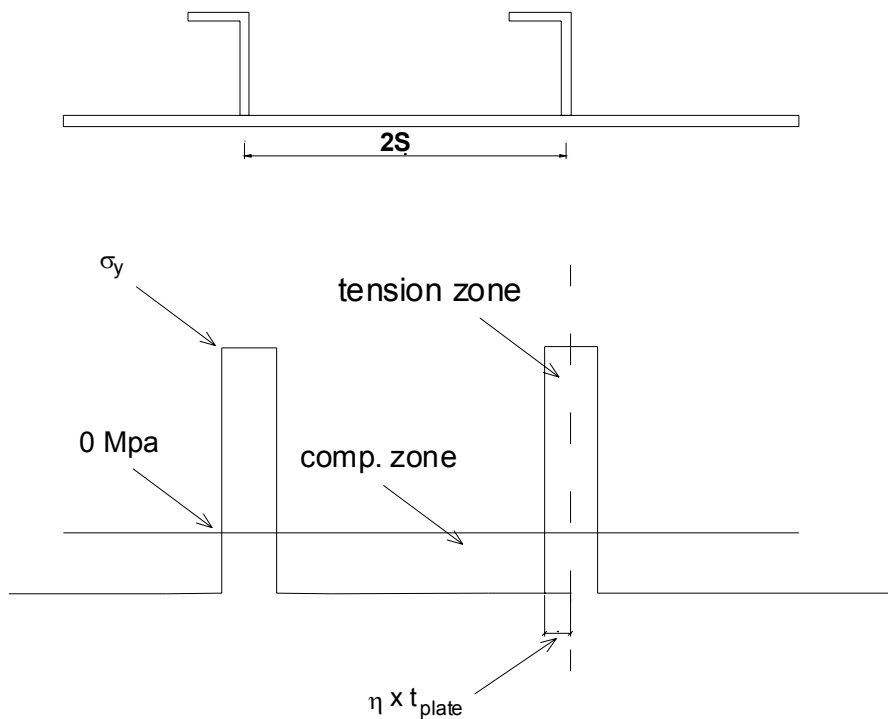
Figure 2-7 Faulkner's model used for residual stresses distribution

2.9   Crack Closure

The closure of a crack could be a result of many factors such as plasticity effect, corrosion products, asperity mismatch, and compressive residual stresses effect. When a crack is undergoing fatigue cycles, plastic deformation at the crack tip induces closure effect on the crack as well as the resistance of plastic strain reversal ahead of the crack

17

tip. Figure 2-8 shows the plastic zone ahead of a crack tip, and the plastic reversal or plastic wake zone. In the case of long fatigue cracks, the plasticity effect is minimal and can be ignored [27].

Corrosion products and asperity mismatch are also regarded as minor effects in the case of long fatigue cracks. However, crack closure from residual stresses has a profound effect on propagation of a crack and must be included in the analysis.

In general, crack closure is incorporated in analytical models or finite element models by computing the values of K_{res}, which is used to calculate the effective K to be used in the crack propagation model used for analysis.

Fatigue tests are often described by their applied stress intensity factor range, or load ratio. The load ratio, or R-ratio, is expressed as:

$$R = \frac{\sigma_{min}}{\sigma_{max}} = \frac{K_{min}}{K_{max}}$$

Equation 2.9-1

Where σ_{max} and σ_{min} are the maximum and minimum applied stresses, and K_{max} and K_{min} are the maximum and the minimum applied stress intensity factors, respectively.
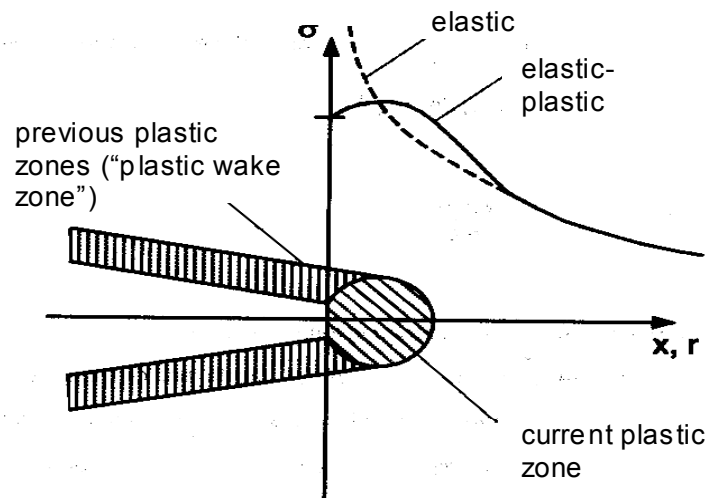
Figure 2-8 Plastic zone formation

18

A crack will only grow when it is opened fully at the tip. So in the case of high compressive residual stresses, a portion of the tensile loading may not contribute to new crack growth and only serves to open the crack. If the tensile loading is not large enough to overcome the magnitude of the compressive residual stresses, then the crack growth could come to a stop. It is good practice to obtain data for crack propagation under high R ratios. This would ensure that the crack is always open, and any effect from compressive residual stresses would be easily identified. Elber [28] has defined the effective tensile loading needed to open a crack by the formula:

$$\Delta\sigma_{eff} = \sigma_{max} - \sigma_{op} \qquad \text{Equation 2.9-2}$$

Where: σ_{max} = the maximum applied stress

σ_{op} = the necessary applied stress to open the crack up to the tip

A ratio describing the effectiveness of an applied cycle was defined as:

$$U = \frac{\Delta\sigma_{eff}}{\Delta\sigma} = \frac{\sigma_{max} - \sigma_{op}}{\sigma_{max} - \sigma_{min}} = \frac{\Delta K_{eff}}{\Delta K_{applied}} \qquad \text{Equation 2.9-3}$$

Where: $\Delta K_{eff} = K_{max} - K_{op}$

K_{op} is defined as the amount of stress intensity factor necessary to open the crack up to the tip along the entire crack front.

3   DESCRIPTION OF EXPERIMENTS

3.1 Test Setup

Although ships are loaded in bending, because of the relatively deep ship section (approximately 30 meters), there is no appreciable stress gradient in a stiffened panel comprising the ship hull. Therefore, it was felt that loading the specimens in tension was more appropriate and representative of the real life situation.

Very limited research has been performed in the past on axially loaded panels because of the large load capacity required to get significant stresses into a large-scale specimen. In this project, a test fixture was specially developed that uses leverage to get up to 2400 kN load on the specimen from a 480 kN actuator.

Figure 3-1 shows the test fixture with a specimen in place. As shown in Figure 3-2, the test fixture was a frame. The top and the bottom of the frame each consisted of four W27 x 84 beams.   The top beams as well as the bottom beams were connected using diaphragms.   These diaphragms ensured that the beams would experience the same displacement, resulting in an evenly distributed load across the panel.   The diaphragms also prevented any relative displacement between the beams.   Eventually, unwanted cracks occurred in the test frame. The cracks in the frame as well as the repair process will be explained in Appendix A at the end of this report.

The left side of the test frame was an actuator that was used to introduce the cyclic loading and to create the tensile stresses on the specimen. The actuator was connected to the top and bottom beams using W 14 x 132 spreader beams (one on the top and one on the bottom). Four columns, W12 x 50, were placed at the right side of the frame to support the top four beams and to create a point of rotation that allows for the fatigue cycles. This point of rotation was introduced by placing a pin connection on the top of the columns. The bottom beams and the columns were fillet welded together. Finally, the test specimen was placed between the actuator and the columns at a distance 2440

mm away from the actuator or 610 mm away from the columns, and connected to the top and bottom beams with high-strength structural bolts, using double angles.

Figure 3-1 Test frame with specimen in place
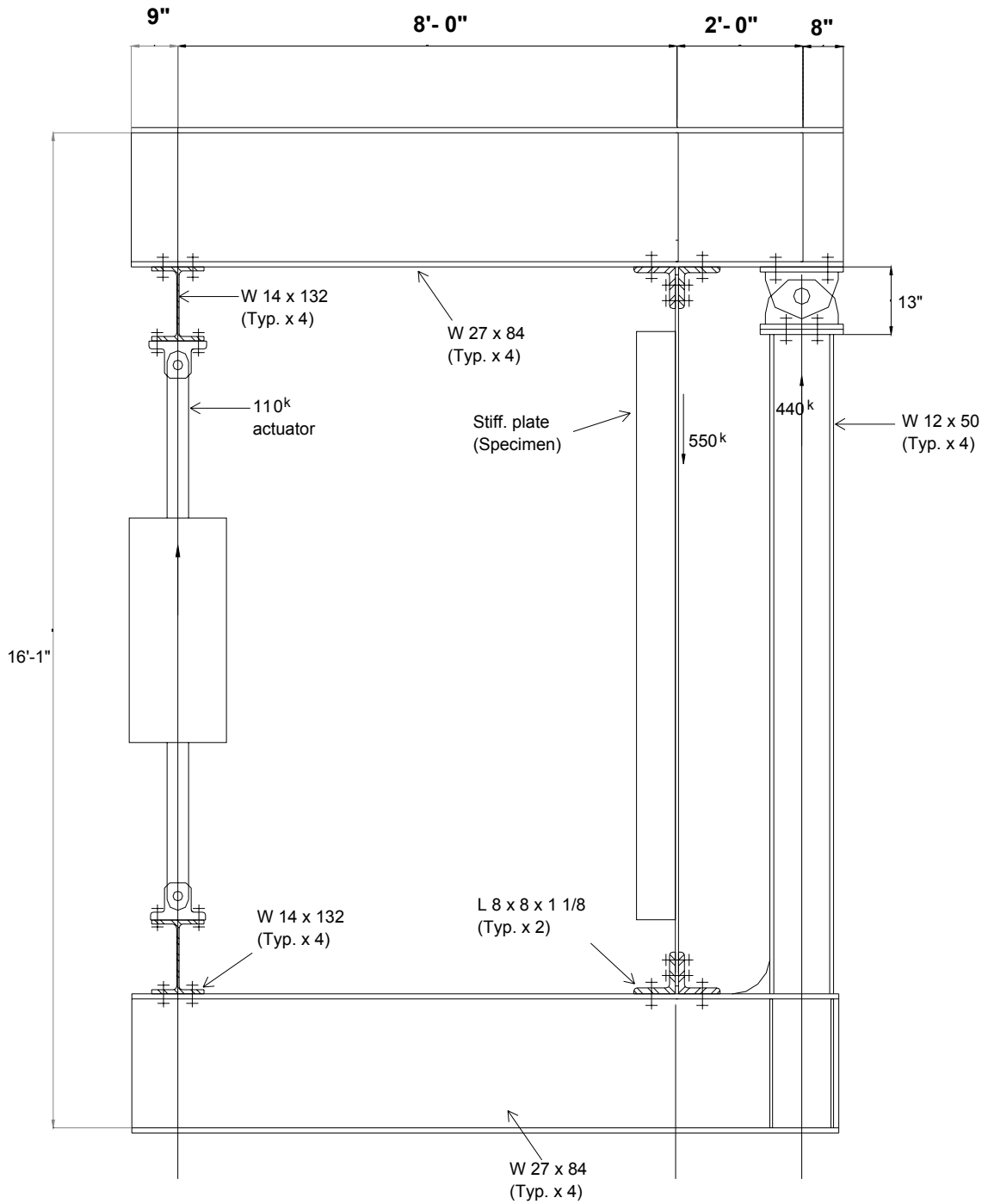
Figure 3-2 CAD drawings for the side view of the test frame

To ensure that bending of the stiffened panel is kept to a minimum, the distance between the edge of the plate and the end of the stiffeners was made long enough, 340 mm, so that

the small amount of bending would be handled by the flexible plate edge without transferring into the stiffened portion of the test specimen.

Unfortunately, the test frame experienced some problems with bolts failing at the connection between the angles and the lower and top beams. To eliminate the problem, two spreader beams were added to the frame, one W 14 x 174 on the top, and one W 14 x 233 on the bottom across the W27 x 84. Threaded rods were used to connect the angles to the specimen. The W27 x 84 beams were no longer bolted to the angles. Figure 3-3 shows the threaded rods connecting the angles to the spreader beams in the modified test frame.
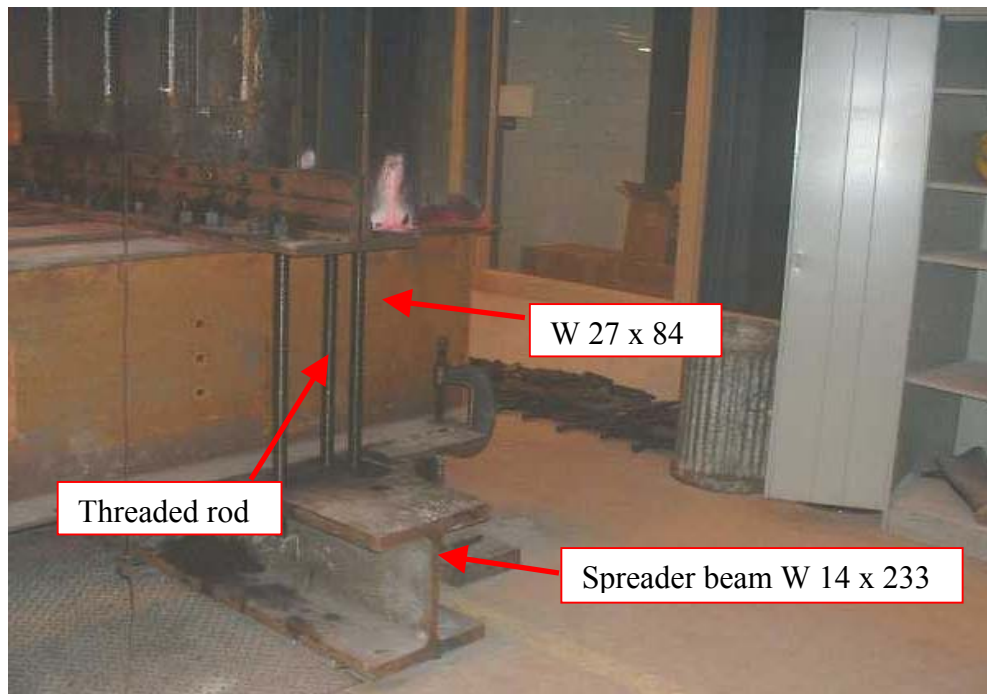
Figure 3-3 Modified test frame setup

3.2 Specimen Fabrication and Test Program

The fabrication of the test fixture and the specimens was done at a local steel fabricator. The plate of the specimen was high-strength low-alloy steel (ASTM designation A572). The bulb-tee stiffeners were HP 160 x 9 and were obtained from Premier Steel Inc. of Englewood, NJ. The "160" and the "9" refer to the length and the thickness of the

stiffener web in mm respectively. The stiffeners were designated as Grade AH36 ship steel. The angle stiffeners were L101 x 76 x 8, made with corrosion resistant high strength low alloy material (ASTM designation A588).

Two different types of specimens differing in their stiffener type, either angle or bulb-tee stiffeners, were fabricated. One plate, which was 1626 mm wide and 13 mm thick, was fabricated with angle stiffeners. The angle stiffeners were 101 mm x 76 mm x 8 mm, with a spacing of 381 mm. Four specimens were fabricated with bulb-tee stiffeners (HP 160 x 9). The thickness of these plates was either 13 mm or 9 mm, with stiffener spacing of either 381 mm or 305 mm. Figure 3-4 shows typical specimen dimensions and the stiffeners' spacing. Table 3-1 lists the test matrix for the specimens tested.
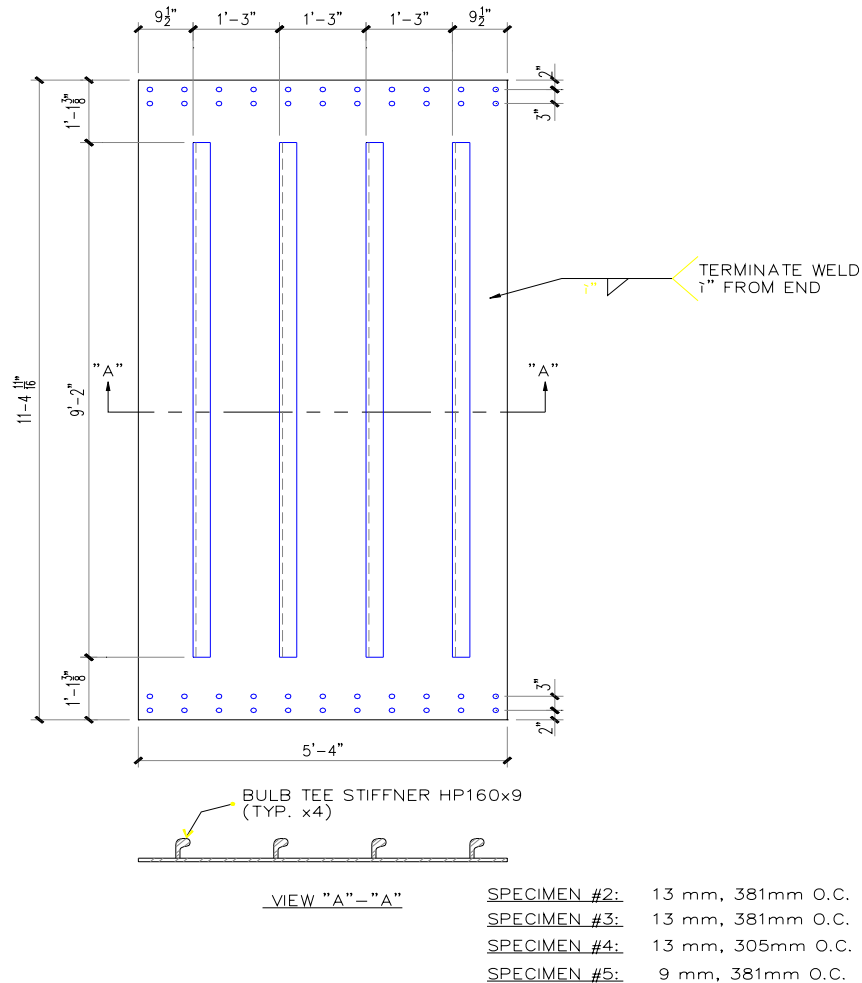
Figure 3-4 CAD drawing of specimen

24

Flux core arc welding (FCAW) was used to introduce the medium heat input used in the welding processes. An electrode size of 1.6 mm was used to obtain an 8 mm single pass weld. The welding current was 265 – 320 A, with a voltage 27 – 31 V, and a travel speed of 254 – 305 mm/min. The filler metal classification was E71T-1 LINCOLN OUTERSHELD 71 and was in accordance with AWS 5.20. Submerged arc welding (SAW) was used to introduce the high heat input.

Table 3-1Test Matrix

Specimen #	Plate Thickness	Type of Stiffener	Stiffener Spacing	Heat Input
S1⁻	13 mm	Bulb tee	381 mm	Medium*
S2⁻	13 mm	Bulb tee	381 mm	High*
S3⁻	13 mm	Bulb tee	305 mm	Medium*
S4⁻	13 mm	101x76x8 angle	381 mm	Medium
S5⁻	9 mm	Bulb tee	381 mm	Medium

* Residual stresses were measured on these three specimens
- Plate in all specimens were fabricated from A572 (f_y = 50ksi)

3.3   Testing Parameters

The type of loading a structure can experience is either load control or displacement control or a mixture of both. Load control occurs when the applied load does not decrease as a result of an increasing flexibility of the system. Ship structures being exposed to waves will always experience the same load regardless of the length of the crack, or the response of the structure. In other words, a reduction in net section will make the structure increase its displacement, but the applied loading remains the same.

On a local scale, the loading experienced by the structure is displacement control. This type exists when adjacent structural members limit the displacement of a cracked member. The adjacent members simply become more stressed while restraining the cracked specimen from displacement. Structurally redundant ships exhibit a great deal of

displacement control behavior due to numerous load paths inherent in the cellular structure. As the crack gets bigger, the cracked component or member loses its ability to carry load and transfers or sheds the load to an un-cracked member. This phenomenon is known as load shedding.

All specimens were tested in tension with a load ratio ($\sigma_{min}/\sigma_{max}$) of 0.2, and frequency of 0.7 hertz. These experiments were conducted under load control. The temperature was held constant at approximately 25^0C (laboratory temperature). Temperature may play a significant role when considering the fracture toughness of the material, which in return will influence the fracture behavior of the plate. However, thin structural steel plates typically meet minimum fracture toughness requirements which are specified at temperatures much below the normal laboratory temperature. For AH36 steel the minimum Charpy V-Notch Impact required is 34 J at 0 ^{o}C, and for EH36 the minimum requirement is 34 J at -40 ^{o}C [29]. Changing the temperature of the specimen between these values would have required special equipment that was not available. The effect of temperature on the fatigue behavior is negligible. Therefore, it was felt that ignoring the temperature effect is reasonable, as the purpose of the research was to investigate crack propagation and not fracture.

The length of the introduced initial cracks was kept constant (305 mm) among the specimens. One specimen was welded with a high heat input since it was believed that the high magnitude of residual stresses induced by welding the stiffeners could have the greatest influence on the growth rate of the crack. However, the measured residual stresses were not substantially different.

3.4   Test Procedures and Initial Measurements (Base Line)

The first specimen to be tested was specimen S1 (refer to Table 3-1 for details). This specimen was used for the shake down processes to get a feeling for the performance of the test frame. Initially the load was cycled such that the stress range in the specimen was 36 MPa with a load ratio of 0.1.

A hole was drilled in the center (mid length and mid width) of the plate and a saw cut was made to introduce a 75 mm long crack. A weld bead was placed at each crack tip to accelerate the initiation of a fatigue crack. After undergoing a total of 490,000 cycles, a fatigue crack still had yet to initiate, and the length of the initial crack was increased to a total of 180mm. Figure 3-5 shows this initial crack in the specimen. Although this crack began to propagate, after about 900,000 cycles the crack had propagated away from the initial weld bead (which created tensile residual stress) and was no longer growing. The initial crack was increased to a length of 305 mm and the stress range was increased to 55 MPa, after which the fatigue crack propagated until failure of the specimen.

The remaining specimens were tested with 305 mm initial cracks with weld beads at the tips and a stress range of 55 MPa and load ratio of 0.2. To distinguish between the cracks propagating on each side of the hole, the crack propagating to the right of the hole when looking at the stiffened side of the specimen is referred to as the "North side" crack, while the one to the left of the hole is referred to as the "South side" crack.
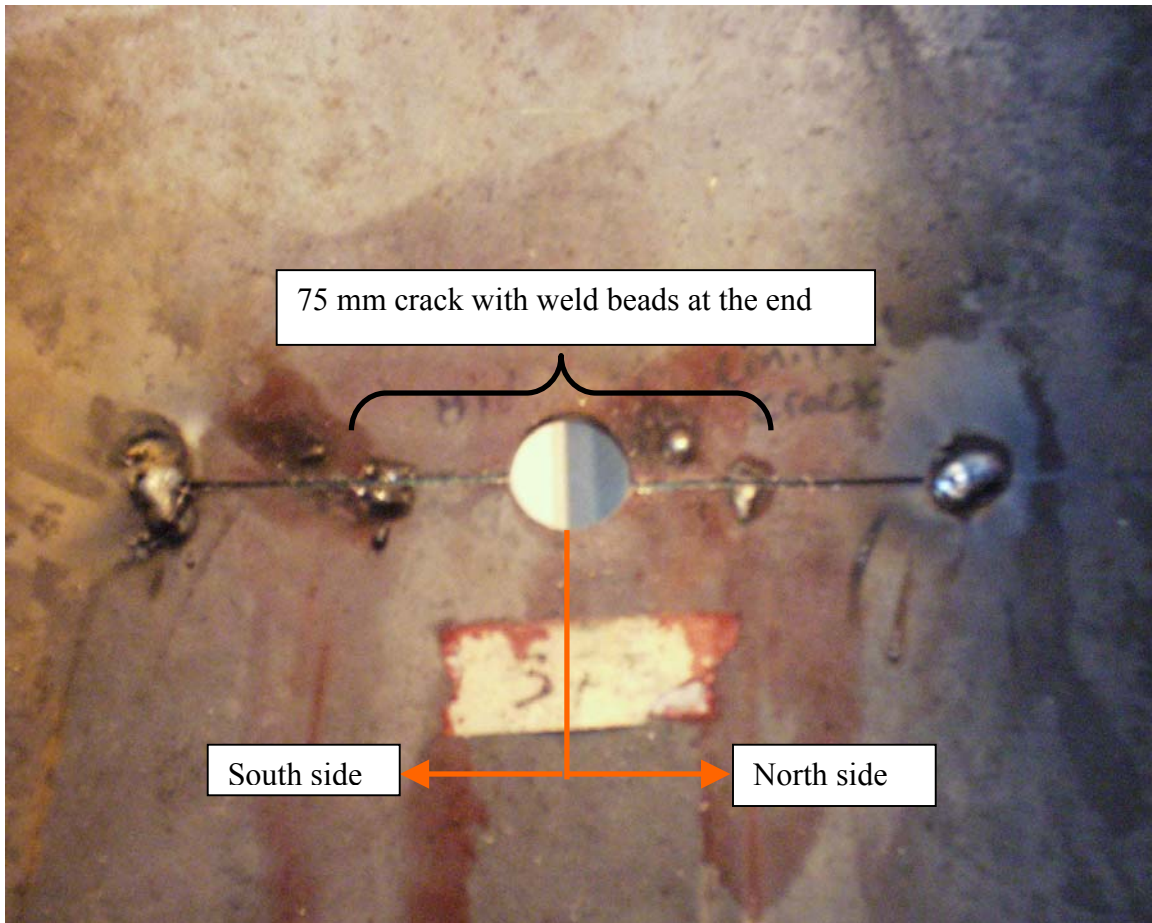
Figure 3-5 Initial crack and weld beads

3.5   Experimental Results

Basic data of half crack extension versus number of cycles were obtained as the cracks propagated in the stiffened panels. Crack length was measured with a fine scale. The location of the crack tip was enhanced with a red dye that penetrates through the crack when it opens and comes back out as the crack closes.

Figure 3-6 shows crack extension versus number of cycles for specimens S1, S2, S4 and S5. For reference, the predicted crack propagation of a center-cracked tension (CCT) plate with no stiffeners is also shown. The data for specimen S3 is shown separately in Figure 3-7 as it had different stiffener spacing than the rest of the specimens.
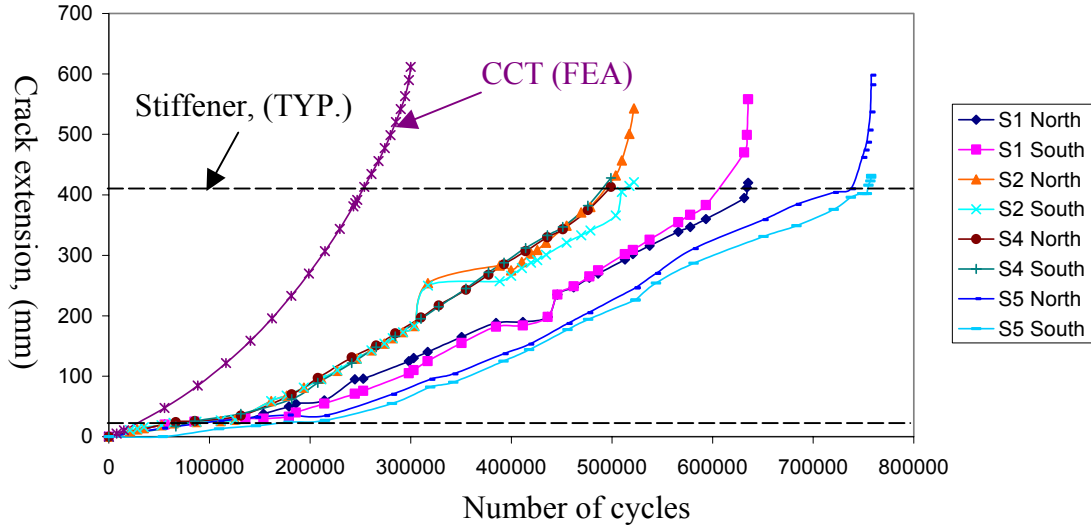
Figure 3-6 Crack Extension versus Cycles for S1, S2, S4, and S5

There is very good agreement between the results of the north and south crack in these experiments. However, there is considerable variation between specimens. S2 and S4 agree very well with each other, which is believed to be coincidence. Note that S2 and S4 have different stiffener types, so this indicates that the type of stiffener is not an important variable. It is not known why S1 and S5 took longer to propagate than S2 and S4, but crack propagation is highly variable as discussed previously. The results could be dependent on a number of factors that were not controlled, such as the sequence in which the stiffeners were welded to the plates. Such variations would be expected to occur in actual ship construction as well. Therefore, an upper bound crack propagation model should be used.
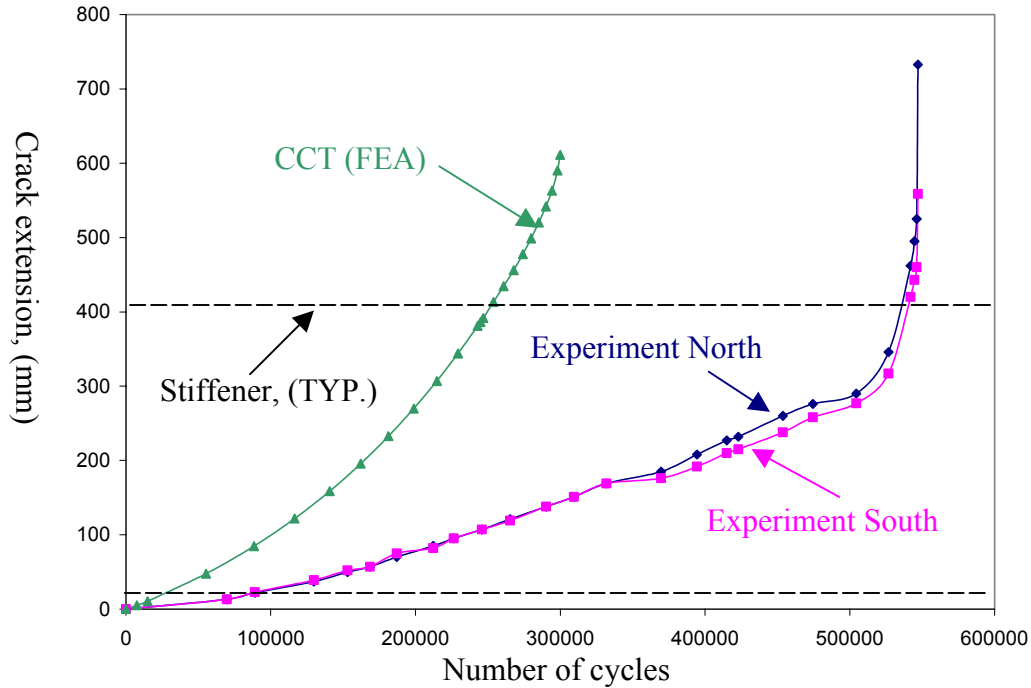
Figure 3-7 Crack extension versus cycles for S3

Dexter and Pilarski's experimental results [6] in Figure 3-8 show that in the case of testing a redundant box section, the number of cycles it took for a crack to propagate between stiffeners is approximately twice as much as the baseline case of a CCT specimen with no stiffeners. This result shows that redundancy and residual stresses were beneficial in slowing the crack propagation rate (decreased by a factor of two).

As can be seen in the results of this project, when testing a single plate with no redundancy, the number of cycles it took to propagate the crack between the stiffeners was also twice as many as in the case of the CCT specimen with no stiffeners. It is important to note that the graph for the CCT specimen in Figure 3-7 was obtained from finite element analysis. The existence of residual stresses increased the number of cycles by a factor of two. Therefore, redundancy had a small effect on the crack growth rate. It is important to keep in mind, however, that while it has little effect on the crack propagation rate, having a redundant structure could be extremely beneficial in keeping the ship intact and preventing break up of the ship as large cracks develop.
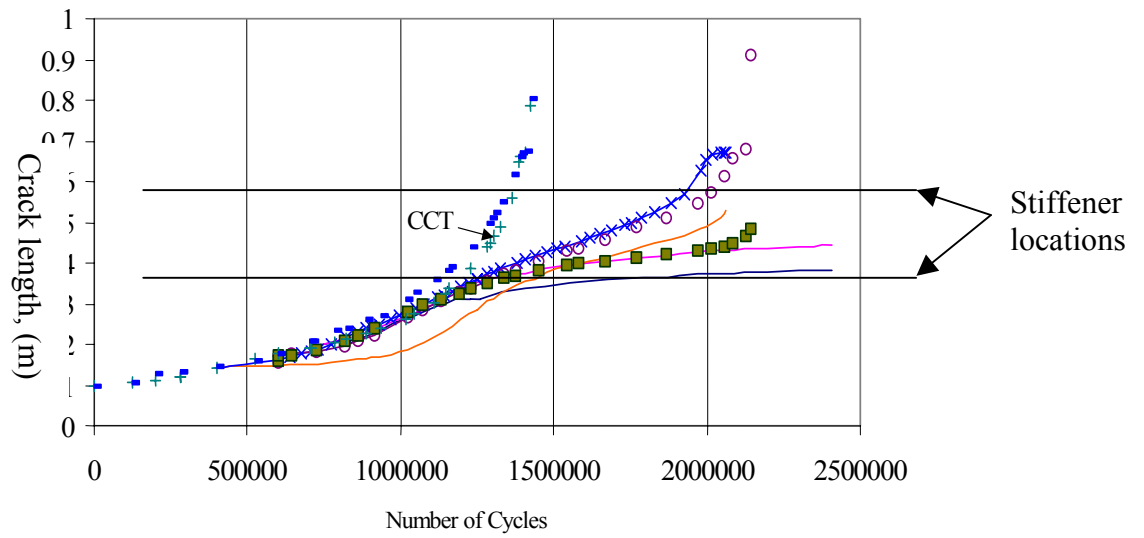
Figure 3-8 Experimental results for crack propagation versus cycles [6]

Table 3-2 lists the crack length in the plates and up the stiffeners for all specimens as well as the remaining sections. Stiffener 1 in the table refers to the first stiffener the crack encounters as it grows (inner stiffener), and Stiffener 2 refers to the second stiffener that the crack propagates through (outer stiffener).

Table 3-2 Final crack extension in plate and stiffeners

Specimen	S1	S2	S3	S4	S5
Cycles count	635,306	521,804	547,126	498,913	757,652
Half crack (Plate north)	420 mm & 232.8 mm remain	543 mm & 109.8 mm remain	652.8 mm & 0 mm remain	412.8 mm & 160 mm remain	598 mm & 54 mm remain
Half crack (stiff. 1north)	145 mm & 15 mm remain	144 mm & 16mm remain	150 mm & 10 mm remain	92 mm & 11 mm remain	108 mm, then severed at 523,221 cycles
Half crack (stiff. 2 north)	34 mm & 126 mm remain	87 mm & 73 mm remain	145 mm & 15 mm remain	10 mm & 91 mm remain	110 mm & 50 mm remain
Half crack (Plate south)	558 mm & 94.8 mm remain	421mm & 231.8 mm remain	478.8 mm & 174 mm remain	427.8 mm & 225 mm remain	432 mm & 212 mm remain
Half crack (Stiff. 1north)	149 mm & 11 mm remain	142 mm & 18 mm remain	152 mm & 8 mm remain	92 mm & 11 mm remain	148 mm, then severed at 523,221 cycles
Half crack (Stiff. 2 south)	90 mm & 70 mm remain	10 mm & 150 mm remain	115 mm & 45 mm remain	23 mm & 78 mm remain	30 mm & 130 mm remain

3.5.1 Specimen S1

As mentioned above, some difficulties in testing were experienced due to unexpected problems with the test frame. Testing of the specimen was completed using the original setup (shown in Figure 3-1), and the data of crack propagation versus number of cycles were recorded. The total number of cycles experienced by S1 was 635,300. Figure 3-9 shows the final crack propagation up the outer South stiffener.

Figure 3-9 Crack propagation for S1 in the plate and the second stiffener (South side)

Figure 3-10 shows that the crack propagated on the North side with a similar rate as on the South side. This observation indicates that the load was evenly distributed across the width of the plate displaying proper functioning of the frame.
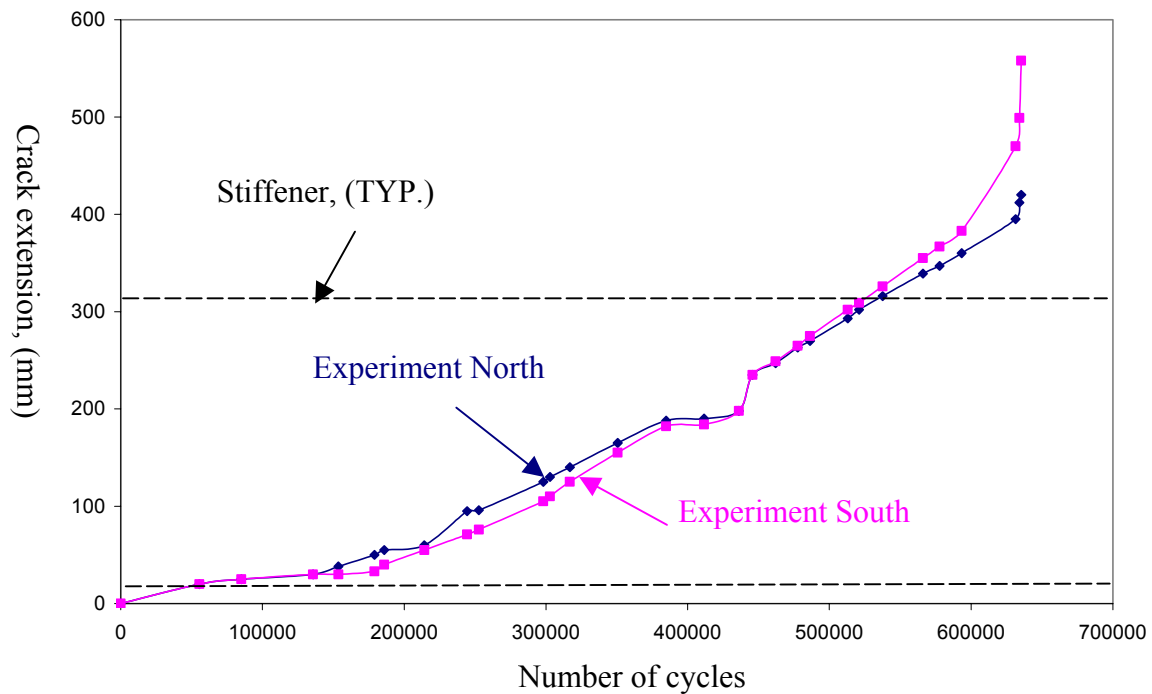
Figure 3-10 Crack extension versus cycles for S1

It was also found that the rate of propagation up the web of the stiffeners was identical to the rate of propagation in the shell plate in all cases until the crack was approximately 80 mm up the stiffener web. Figure 3-11 shows that the rate of propagation in the stiffener was similar to that of the plate up to 250,000 cycles. Beyond that point the rate of propagation up the stiffener became slower than that of the plate. This behavior is attributed to the stress gradient that existed in the stiffener's web. The finite element results in Figure 3-12 shows the stress gradient that caused the crack propagation rate in the stiffener to slow down.
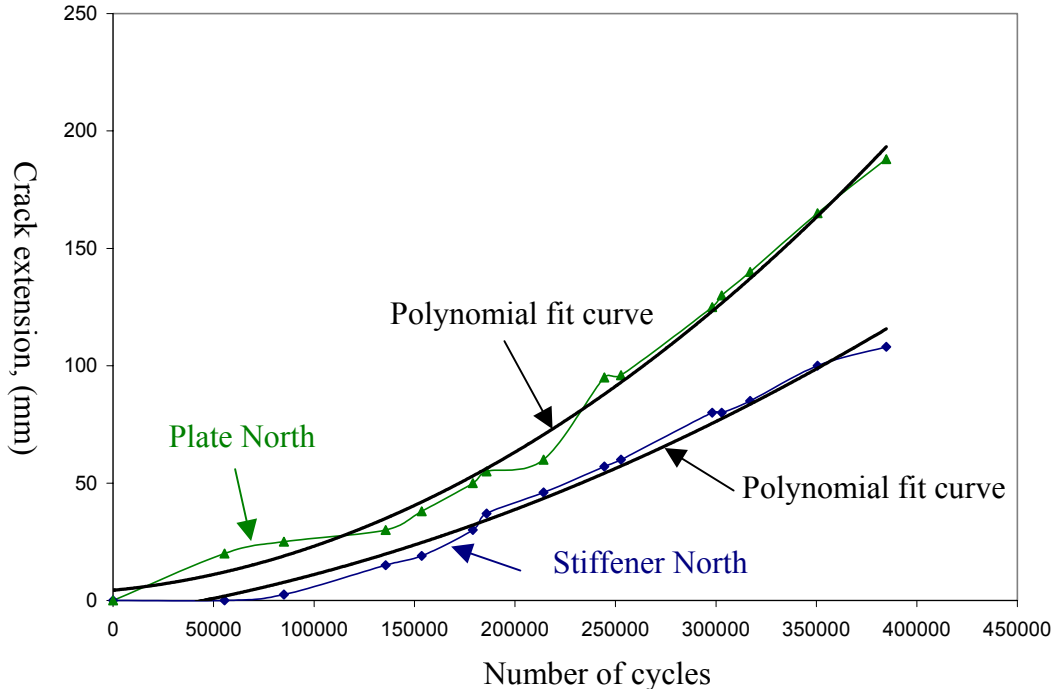
Figure 3-11 Crack propagation rate in the plate and the stiffener for S1
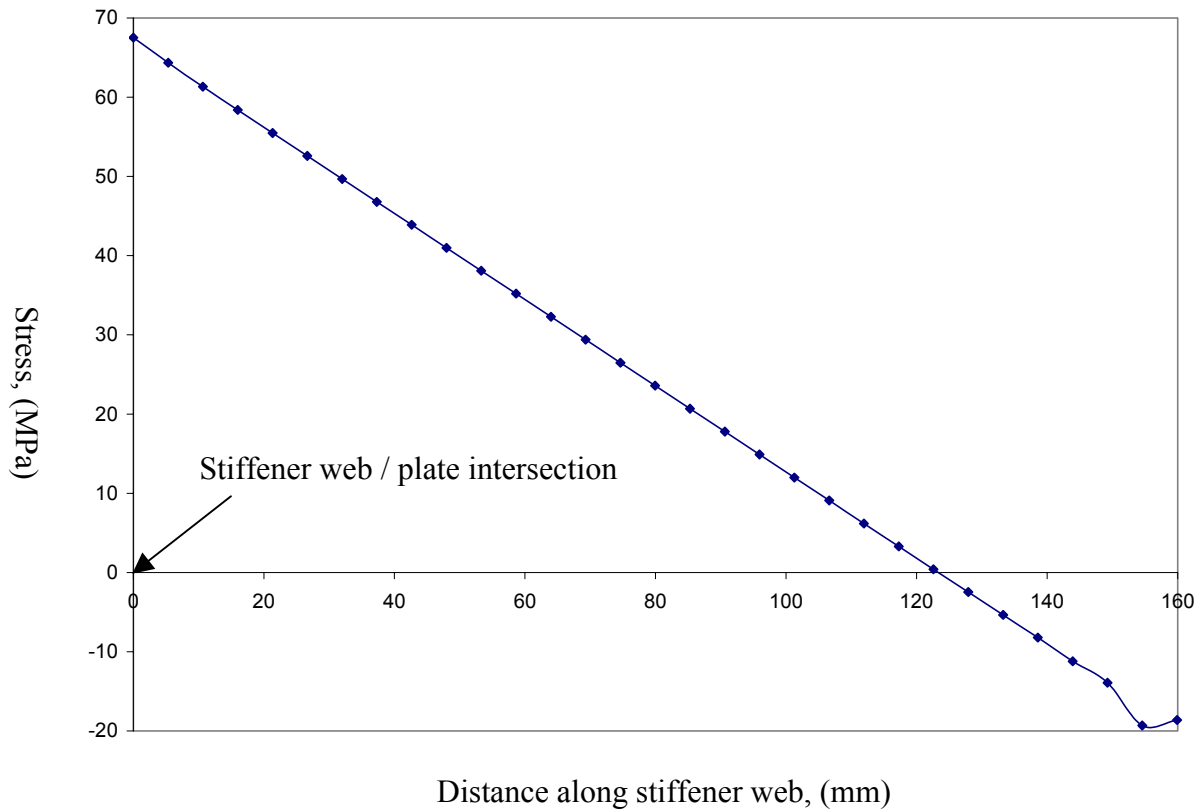
Figure 3-12 Stress gradient in stiffener web using FEA

3.5.2 Specimen S2

Testing of specimen S2 was completed using the modified test frame of Figure 3-3. The total number of cycles it took to fail the specimen was 522,670 cycles. There was a 20% difference in the propagation rate between S1 and S2. Specimen S2 was welded using a higher heat input, which if it had any effect at all should slow the rate of growth rather than accelerate it. As shown in Section 3.6, there was no appreciable difference in the residual stress and therefore this factor is not thought to have influenced the results at all.

Figure 3-13 shows crack propagation versus number of cycles for S2. The propagation of the crack on the north side and the south side was identical up to 340,000 cycles. After that, the south side crack started to fall behind the north side crack, and propagate at a slightly slower rate. The total number of cycles that the specimen underwent was

522,700. It is interesting to note that when the cycle count was around 300,000, there was a jump in the crack propagation followed by a flat curve up to 400,000 cycles, indicating that the propagation was very slow. This is opposite to what happened in specimen S1 where the curve was flat then a jump occurred in the crack propagation.
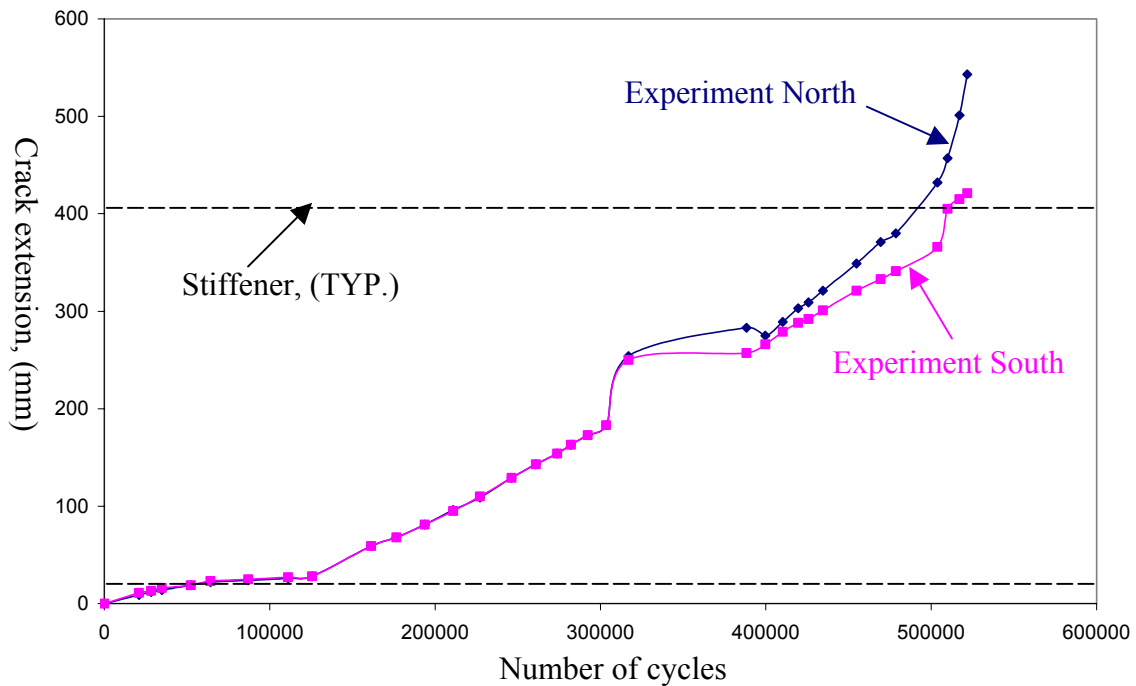
Figure 3-13 Crack extension versus cycles for S2

Figure 3-14 shows the final crack size in the north side of the plate, with a plastic zone forming at the crack tip. A white developer was sprayed on the plate ahead of the crack which flaked off as the plastic zone was forming.

Figure 3-14 Plastic zone forming at the crack tip

3.5.3 Specimen S3

This specimen S3 underwent a total of 547,126 cycles. The crack was left to propagate across the whole width of the plate and started to turn after it passed the second stiffener on both sides of the plate. Turning of the crack started when it was 354 mm long on the north side and 295 mm long on the south side (20 mm passed the second stiffener). The crack underwent a sharper turn in a 20° angle with respect to the horizontal axis with observed benchmarks at the crack surface, indicating a fracture mode of failure rather than fatigue in which the crack propagates perpendicular to the maximum shear stresses. Figure 3-15 shows the final crack as well as the crack turning phenomena.

Figure 3-15 Final crack length and crack turning

The effect of stiffener spacing on the propagation of the crack could be seen when comparing specimen S2 with specimen S3. Both specimens had the same geometry with the exception that S2 had greater stiffener spacing. Both specimens were tested using the same setup. Considering the same final crack length, specimen S3 experienced approximately 25,000 more cycles than specimen S2.

Specimen S3 could have higher compressive residual stresses than the other specimens. The tensile residual stresses in all specimens have about the same magnitude and occupy the same area regardless of the spacing between the stiffeners. However, the magnitude of the compressive residual stresses that form in the region between the stiffeners must equilibrate the tensile stresses. This magnitude will vary based on the spacing between

the stiffeners to ensure that equilibrium state is met. Higher compressive residual stresses will form if the spacing is smaller. Figure 3-16 shows crack propagation versus number of cycles for both the north and the south side cracks.
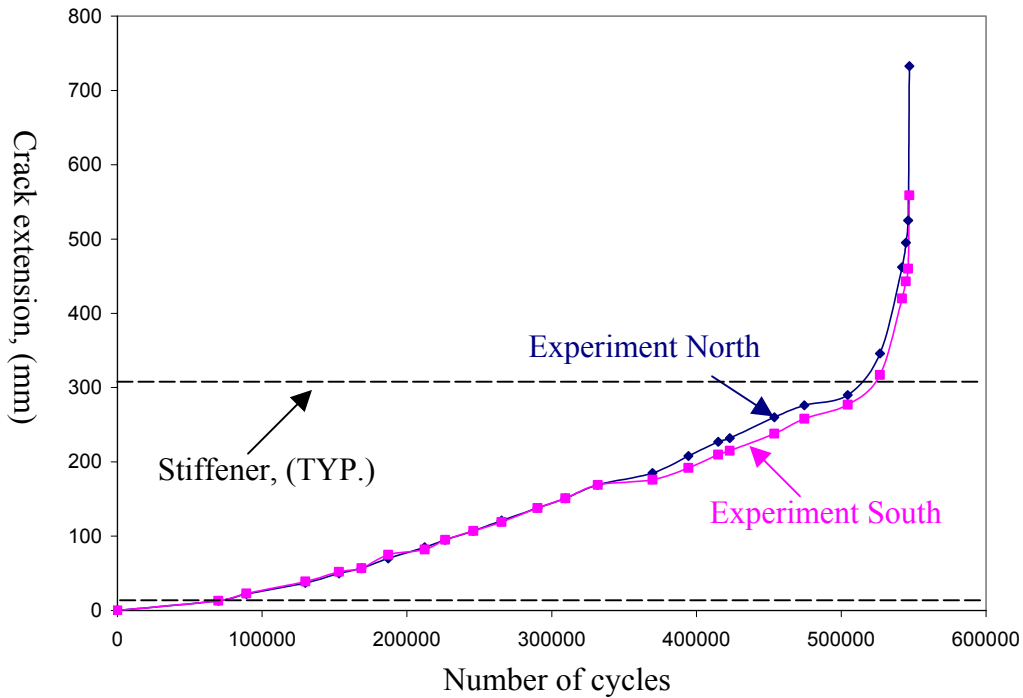
Figure 3-16 Crack extension versus cycles for S3

3.5.4 Specimen S4

The stiffener type did not make a significant difference in the propagation results. The propagation rate for specimen S4 with angle stiffeners was the same as for specimen S2 with bulb-tee stiffeners as can be seen in Figure 3-6.

Figure 3-17 shows the crack propagation rate for both the north and south sides of specimen S4. Since it was observed that the propagation of the crack in S4 was similar to that of S2, testing of S4 was terminated before the crack propagated to the end of the plate.
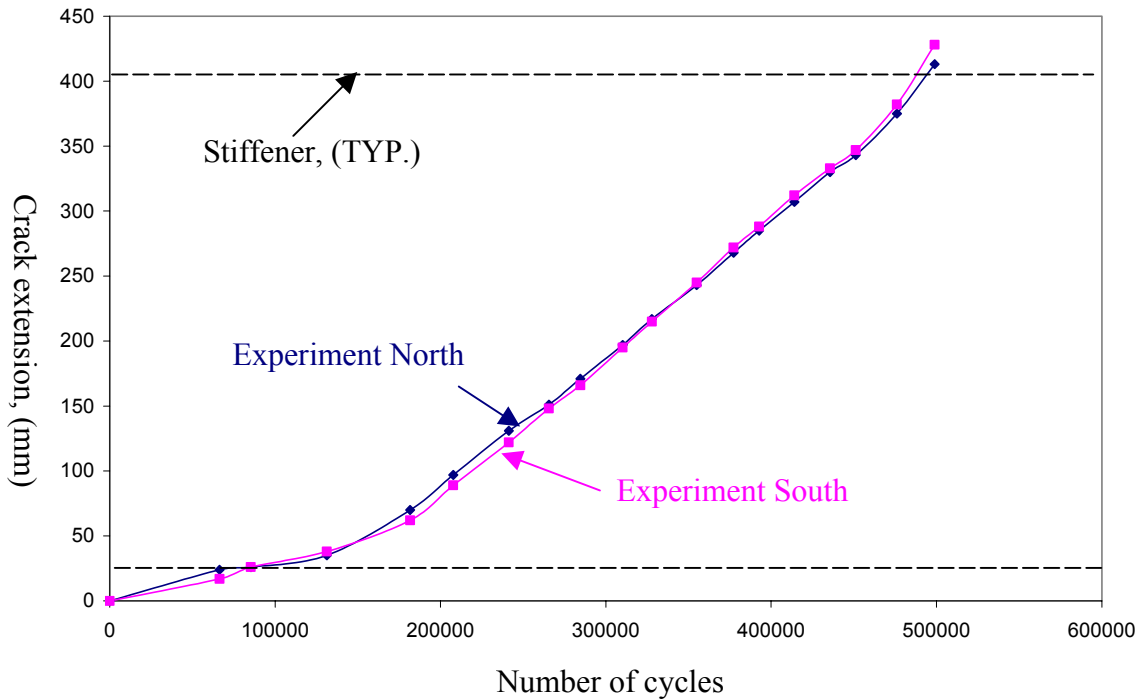
Figure 3-17 Crack extension versus cycles for S4

3.5.5 Specimen S5

Since the plate thickness of specimen S5 was less than the other four specimens, 9 mm versus 13 mm, a reduced load range was used during testing to produce a stress range in the plate consistent with the previous tests. Specimen S5 underwent 757,652 cycles prior to failure, which is more cycles than any of the other specimens. Compared to specimens S2 and S4, which have similar stiffener spacing as S5, the thinner S5 withstood approximately 1.45 times as many cycles before the second stiffeners were breached than the other two specimens. This difference may be due to the effect of plate thickness. It would be expected that the thinner plate with the same size stiffeners would have higher compressive residual stresses, and thus lower crack propagation rate. It is interesting that the stiffeners were intentionally severed in this test to see if this would accelerate the crack propagation, which it apparently did not.

41

As shown in Figure 3-18, the crack grew at a similar rate in the north and south directions. The south crack initiated after the north crack, and thus the south crack lagged behind the north crack slightly throughout the entire test. As was seen in specimens S1, S2 and S3, once the second stiffener was breached, the crack propagation rate greatly increased.
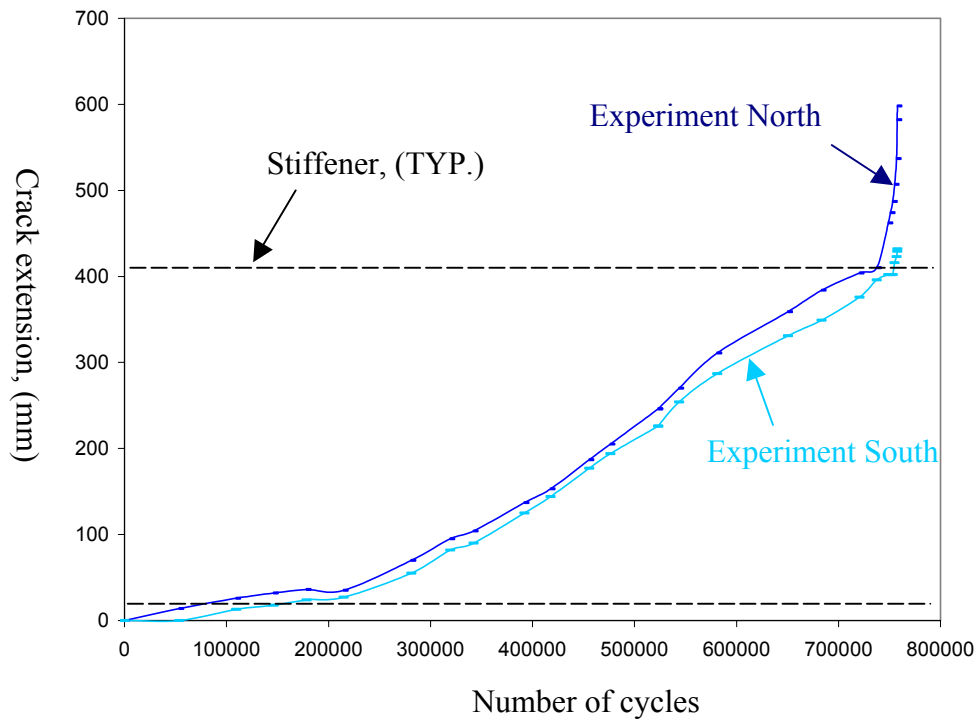
Figure 3-18 Crack extension versus cycles for S5

3.6   Residual Stress Measurements

The measurement of residual stresses was done on specimens S1, S2, and S3 using the sectioning method. S1 was sectioned using 41 coupons with a nominal gage length of 254 mm. Four coupons from either side of each stiffener were taken with a width of 12 mm. Three additional coupons with a width of 37 mm were taken from the region between stiffeners. S2 and S3 were sectioned using a lesser number of coupons with a nominal gage length of 100mm.

The method of sectioning was chosen to be the most economical and convenient method for measuring residual stress. A comparison study between various techniques of residual stresses measurements showed that the sectioning method yields the most accurate results with standard deviation of $\pm 10\,\mathrm{MPa}$, when measured in a normal case [25].

Before sectioning the plate, the gage points were drilled through the thickness of the plate at the center of the sections marked on the plate using a 3 mm diameter drill bit. It was believed that the inherent bending in the plate would have an effect on the measured values, and could possibly result in overestimating the residual stresses. Therefore, drilling a hole all the way through the plate allowed for the measurements to be taken from each side of the plate at the exact same location on the extracted section.

A digital Whitmore gage with accuracy to 0.001 mm was used to measure the distance between the gage points. Three readings were taken on each side of the plate and the average of each three was used. The average of both sides of the plate (the stiffener side and the non-stiffener side) was used to obtain the residual stresses. After recording the initial readings, the plate was sectioned into coupons. The coupons were extracted from the larger section using a band saw that was cooled with a steady flow of cutting fluid. The coolant fluid was applied to prevent any heat input into the plate that might be introduced through the cutting process. After removing the coupons, the final readings were obtained by averaging three readings for each side and then averaging the results of both sides. Figure 3-19 shows the sectioned portion of specimen S1.

254 mm x 37 mm coupon /w
drilled gage point
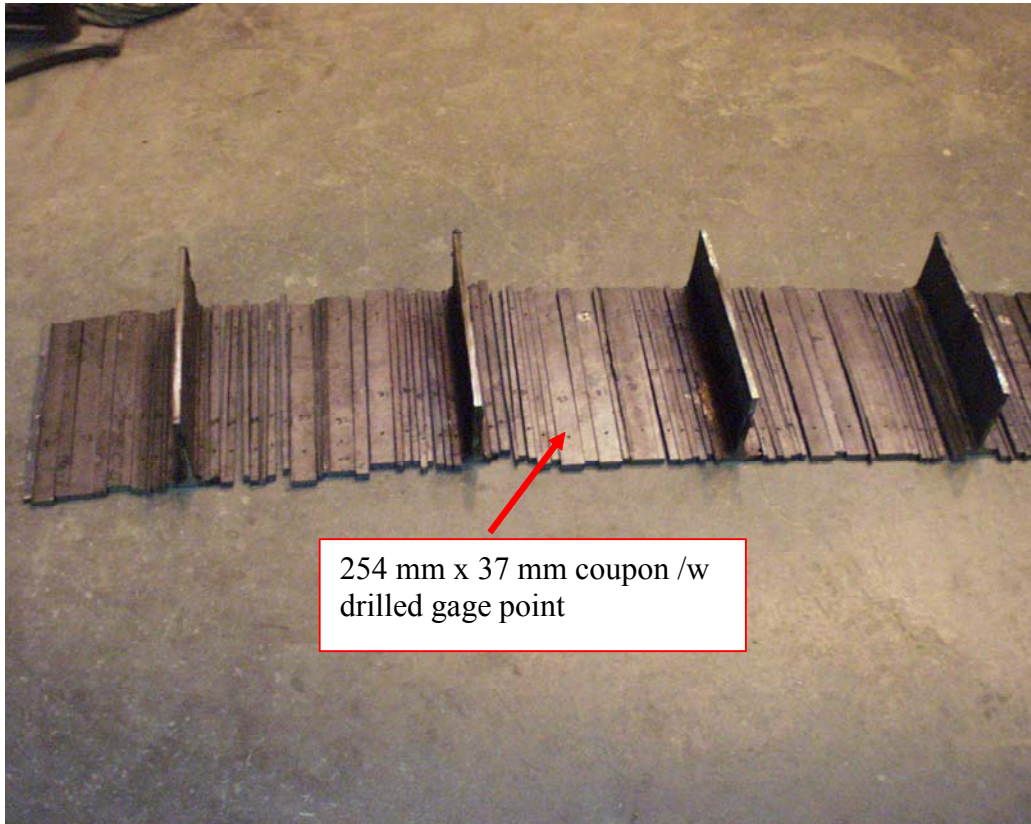
Figure 3-19 Sectioned coupons used for measuring residual stress distributions in S1.

The portion of the specimen used to extract the sections was laid on its flat side, and the saw was dropped on the side that included the stiffeners. The stiffeners' flanges were removed after all the sectioning was done to allow for cutting close to the weld line. At the weld lines the value of tensile residual stresses was assumed to be 350 MPa in the case of specimen S1.

In specimen S2, holes were also drilled through the stiffeners' webs to measure the actual values of residual stress rather than estimating them. A change in length was not detected, however. Therefore, the tensile residual stress value was assumed to be 450 MPa (slightly higher than the value measured in the adjacent strip). It was believed that a change of length was not detected for the strip containing the stiffeners because the error

of measuring the change of length in the strip increases as one moves away from the actual strip.

As expected, some scatter existed in the measured values of the residual stresses. In specimen S1, the values of the measured compressive residual stresses were between 50 and 100 MPa. For equilibrium to take place, assuming that the tensile residual stress is 350 MPa at the weld, a constant compressive residual stress value of approximately 75 MPa must be the actual value present in the plate. This assumption was verified in the F.E analysis as it shows that an assumed value of 75 MPa would yield a very similar behavior for crack propagation as was seen in the experiment.

More scatter in the measured values was observed in specimen S2 than in S1. It is unclear why there is more scatter in the measured values in S2 considering that the steps taken were identical.

Faulkner's model for residual stress distribution was utilized as a simple representation of the actual residual stress in the specimens. This model, as discussed in section 2.8 models the tensile regions around the stiffeners as rectangular shapes with a base width proportional to the plate thickness. The rectangular width typical of as-built ship structures ranges from 3.5 to 4 times the plate width, while values between 3 and 3.5 are more typical of ships after shakedown. The analytical program developed by Dexter and Piliraski [6] includes a routine for developing the Faulkner representation based on the yield strength of the material, the plate thickness and η. Figure 3-20 and Figure 3-21 show the typical residual stresses measured in the plates for specimens S1 and S2, and S3, respectively.
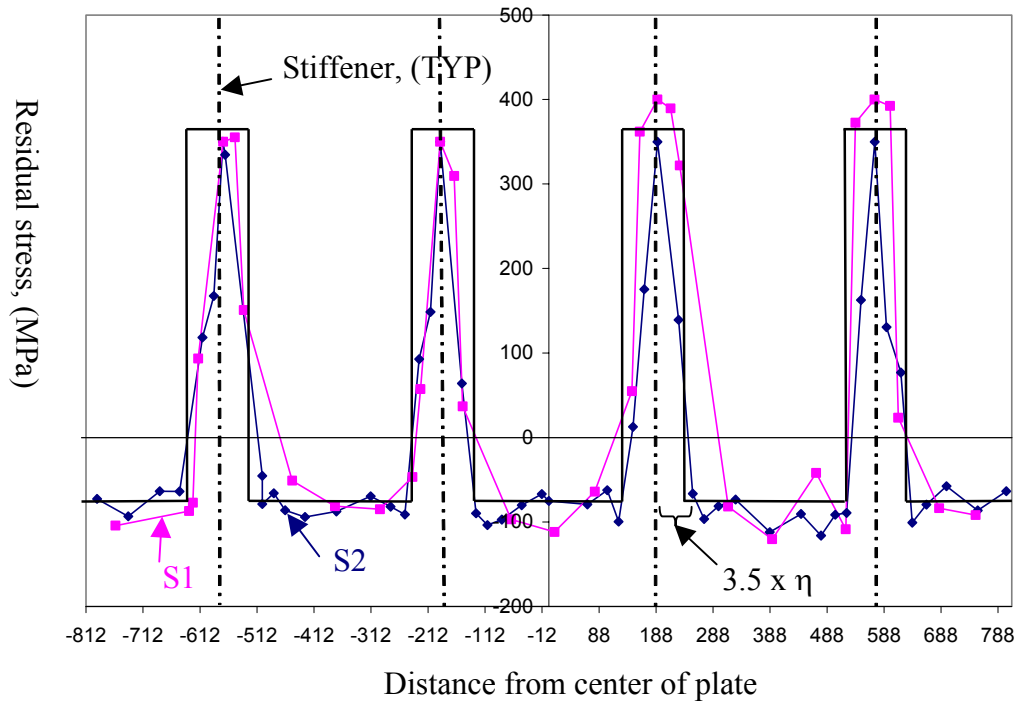
Figure 3-20 Residual stresses measurements in S1, and S2
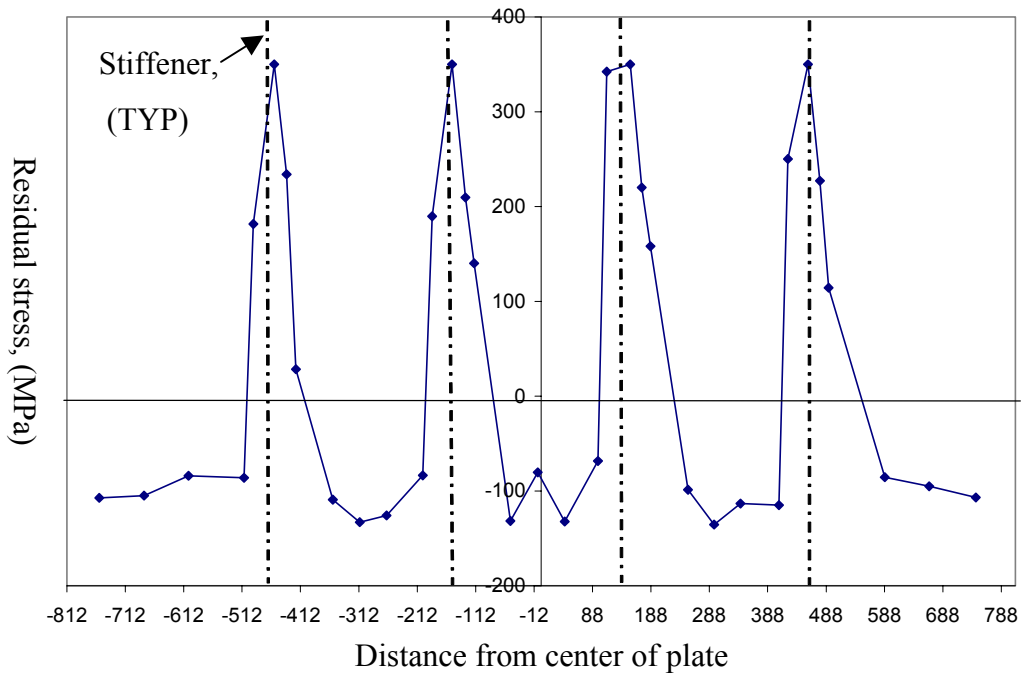
Figure 3-21 Residual Stresses Measured in S3

Even though the values of the measured residual stresses are not in equilibrium (i.e. the area under the compressive zone is not equal to the area under the tension zone), the values seem to be symmetric. The scatter in the measured values was expected, but not accounted for in the finite element analysis.

4 FINITE ELEMENT ANALYSIS

4.1 Introduction

Finite element analysis was used as a tool to investigate the crack propagation in the stiffened panel. Generally, static analysis of stress intensity factors is used to determine the crack propagation rate by comparing the critical value of the stress intensity factor K_{IC} to the K value associated with a specific crack length. The static analysis could be done many times to obtain K for various crack sizes. These values are then used to determine the number of cycles required to propagate the crack a distance da.

 Top-down analysis for an entire ship could also be used. It considers the global response of the ship as a whole, and correlates that response to the local response of a certain structural component of the ship. Spectral analysis is used to incorporate the loading of the ship as well as the speed to obtain the global response of the model, from which the local response could be correlated. From such information, the static analysis of stress intensity factor could be used to determine the required number of cycles for the crack to reach a certain length. Obviously, this method is useful for investigating a particular case, which requires obtaining the data of the loading and the speed for a particular ship configuration.

In this project, K values associated with certain crack lengths were obtained. For a specified direction cosine of the crack as well as the node number at the crack tip, the J–Integral values were computed, and then converted to K values using Equation 4.1-1.

$$K = \sqrt{JE} .$$

Equation 4.1-1

> where: J = the J-integral
>
> E = Young's Modulus

The values of $K_{app, max}$, $K_{app, min}$, and K_{res} were found by running the analysis for every load case separately, then using superposition ΔK_{eff} required for the Paris law equation

was determined. When running these analyses, one must be careful not to apply $\Delta\sigma$ to the plate and find the ΔJ, then convert the value to ΔK, as J and K do not have a linear relationship.

4.2   J-Integral Background

The J-Integral is a fracture characterizing parameter equivalent to energy release rate in non-linear elastic materials. It was presented by Rice [30] as a path independent contour integral for analysis of cracks. Mathematically, J is obtained by evaluating an integral around a path containing the crack tip [31].

That is,

$$J = \int_{\Gamma} (W dy - T_i \frac{\partial u_i}{\partial x}) ds = -\frac{\partial V}{\partial a}$$ *Equation 4.2-1*

> Where: Γ = the contour path, depicted in Figure 4.1
>
> W = strain energy density
>
> T_i = components of the traction vector which is normal to the contour
>
> u_i = components of the displacement vectors
>
> ds = length increment along the contour Γ

This integral is basically the change in potential energy associated with the virtual crack extension, *da*.
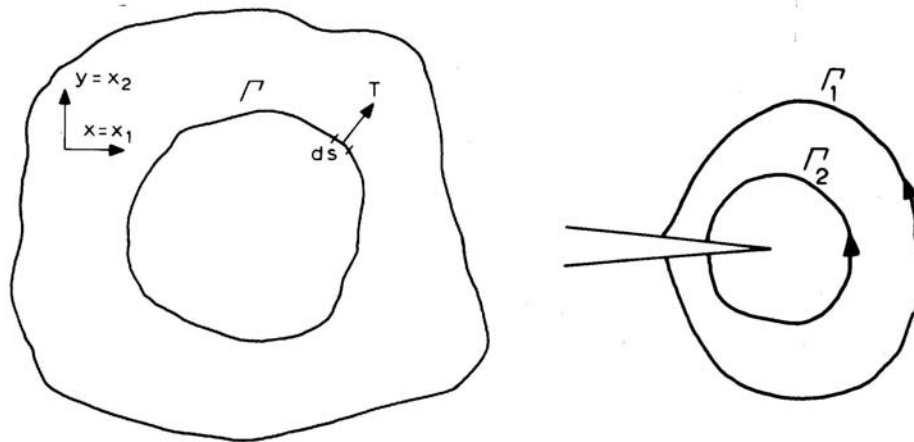
Figure 4-1 Contour path used for J evaluation

The finite element method evaluates Equation 4.2-1 for a specified node, i.e. the node representing the crack tip, by computing the strain energy density W.

$$w = \int_0^{\varepsilon_{ij}} \sigma_{ij} d\varepsilon_{ij} \qquad \textit{Equation 4.2-2}$$

Where, σ_{ij} and ε_{ij} are the stress and the strain tensors.

The calculation of J is path independent, which means any chosen path should yield the same value of J as long as it encircles the crack tip. The obtained value of J relies on the calculated values of the stress and the strain for the elements on the contour surrounding the crack tip. Therefore, one must be careful when meshing the plate to assure correct values of calculated stresses and strains

4.3 Numerical Model Development

A 3-D analysis was performed using "ABAQUS" Software, which was available through the University of Minnesota Super Computer Institute. Because of symmetry, only 1/4 of

the plate was modeled, which helped in reducing the time required for analysis significantly. One must be careful when applying the uniform load to the edge of the plate. The uniform traction does not produce the same force on each node on a quadratic edge. That is, the edge nodes of an element should be assigned 1/6 of the load, while the middle node takes 2/3 of the load [32]. Because of the possibility that one could make an error when assigning these load ratios, it was found to be easier and less confusing to apply displacements at the end of the plate. In this case, the displacement assigned would be equal for each node. Whether it is load or displacement that is being applied, the final stresses seen by a particular element should be the same in both cases. These stresses corresponded to the stresses measured in the laboratory using strain gauges.

Since a high stress gradient existed between the region of compressive residual stresses and tensile residual stresses, it was felt that using eight node quadrilateral shell elements with reduced integration would be appropriate to better capture the stresses. In general, the total number of elements varied between 9000 and 11000 elements per specimen. At plate intersections, ABAQUS automatically uses shell elements with full integration. A typical mesh size used for the analysis was 5 mm at and around the crack face region. Figure 4-2 shows the mesh size as well as the boundary conditions used for the analysis.
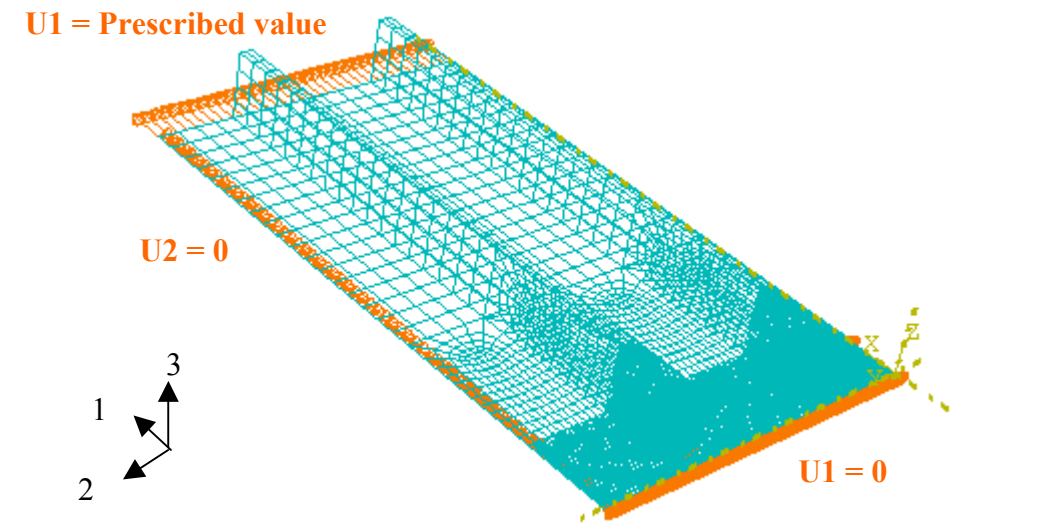
Figure 4-2 Typical mesh & boundary conditions

4.4   Stress Intensity Factor Evaluation Method

To determine the value of the J-Integral associated with the new crack length, boundary conditions in the form of constraints were introduced at the crack face, and released to propagate the crack a distance da. For each crack length, three different values of the J-Integral were calculated and obtained from the output file.   Each of the three J values was calculated by evaluating an integral on an independent path surrounding the crack tip. An average of only the second and the third values was computed. This is because inaccuracies in the stresses at the row of elements immediately adjacent to the crack tip could yield higher error than subsequent contour paths. Equation 4.1-1 was then used to calculate the stress intensity factor K_{app}, or K_{res}. As mentioned before, one must conduct a meshing study, as having a very coarse or very fine mesh size could yield an inaccurate J-Integral value. This is especially true when calculating the K_{res} because of the large stress gradient at the transition area from tensile to compressive residual stresses. A mesh study for this model was conducted by comparing the solution of a center crack tension panel with no stiffeners using equation 2.4-3 to the finite element solution of the same panel.

Barsoum and [33], introduced singularity at the crack tip by moving the mid-side nodes adjacent to the crack tip to quarter points. Nussbaumer [21] found that models analyzed without introducing singularity showed a small difference with comparison to the models with singularity. That difference was 5% on the first contour and 1% on the second contour. It was therefore unnecessary to reproduce singularity in our model since the value of the first contour was disregarded and the value of the second would only exhibit 1% difference.

4.5   Residual Stresses Modeling

The stresses were introduced in the plate by specifying initial tensile stresses in a region equal to $\eta * t_{plate}$, where η is equal to 3.5. This value represents the tension block suggested by the Faulkner model. The stresses were specified in the desired local direction for the selected elements.   The compressive residual stresses were then

52

generated in the analysis to satisfy equilibrium. Figure 4-3 shows the distribution of the tensile and compressive residual stresses in the stiffened plate.
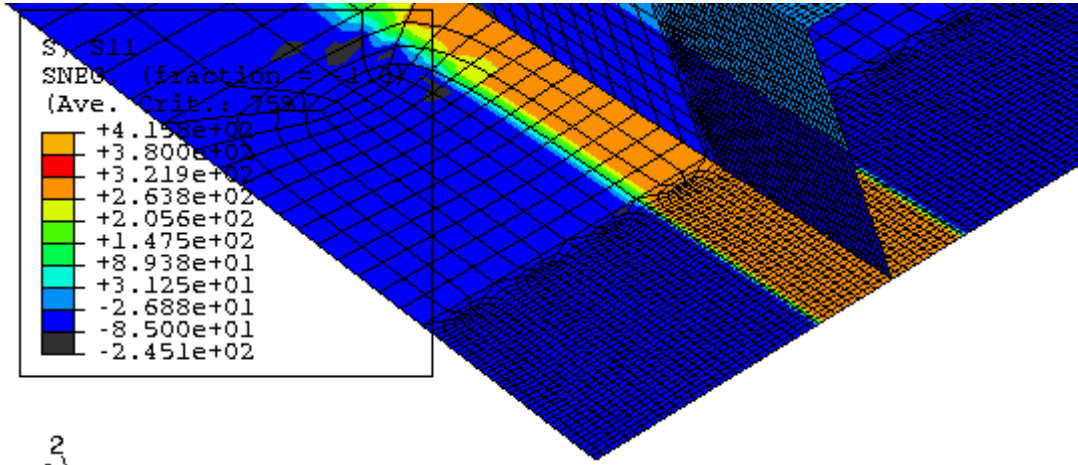
Figure 4-3 Typical residual stresses in the plate

Because there was quite a significant scatter in the measured values of residual stresses, it was desirable to see the effect of the magnitude of these stresses on crack propagation. This was done by conducting the analysis three different times using compressive residual stresses values of 50, 75, and 100 MPa. These values were chosen as they approximately represent the minimum, average, and maximum measured values in specimen S1. The values of K_{res} were calculated the same way as K_{app}. The nodes were released to propagate the crack to the desired length, allowing for the redistribution of residual stresses.

The effect of the magnitude of the compressive residual stresses on ΔK_{eff}, could easily be seen in Figure 4-4 and Figure 4-5. The gap between ΔK_{app}, and ΔK_{eff} in the case of – 100 MPa is higher than the case of –50 MPa. Obviously, as the magnitude of the compressive residual stresses goes to zero, both lines should merge, and ΔK_{eff} would be equal to ΔK_{app}. This comparison shows how sensitive the analysis is to the magnitude of the residual stresses.

Nussbaumer [21] and Thayamballi [18] agreed that the effect of redistribution of the residual stresses was minimal and insignificant. This was proven to be the case in this project as well. Figure 4-6 clearly demonstrates that the redistribution of residual stresses as the crack propagated across the panel is quite small.
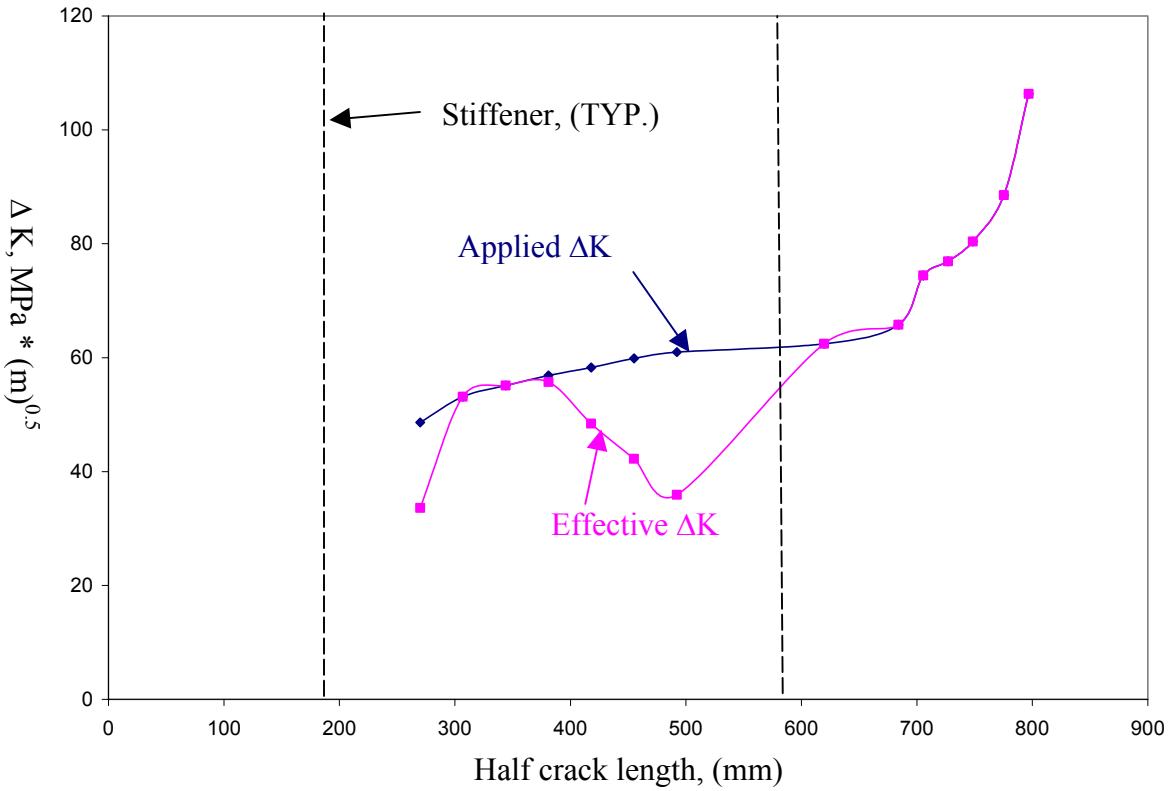
Figure 4-4 ΔK_{app} & ΔK_{eff} for compressive residual stresses of 100 MPa
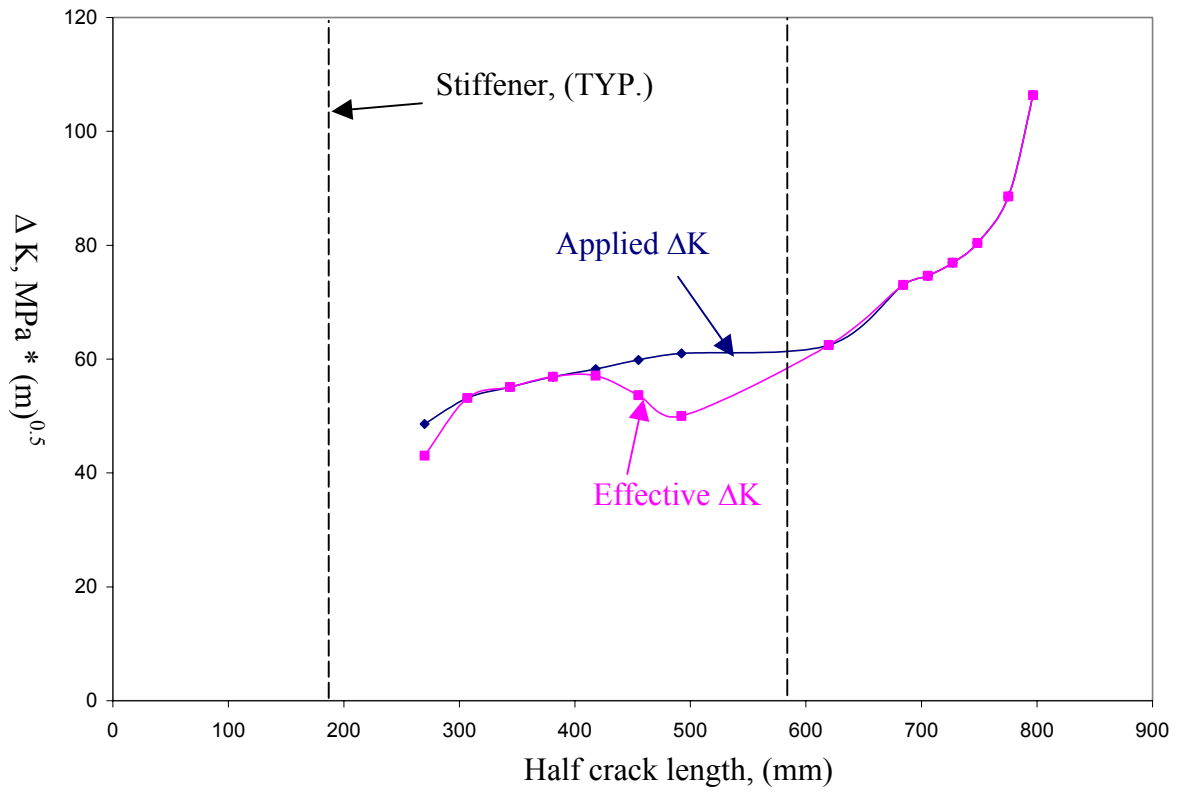
Figure 4-5 ΔK_{app} & ΔK_{eff} for compressive residual stresses of 50 MPa
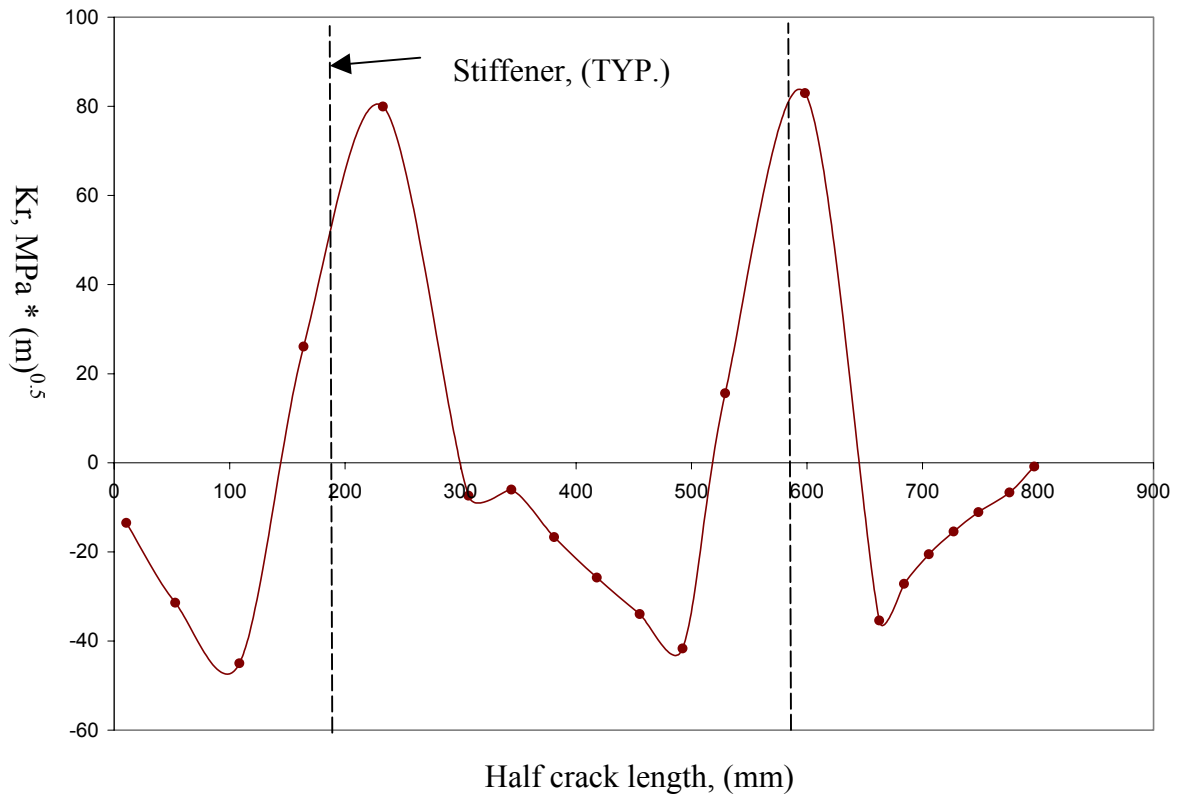
Figure 4-6 K_res calculated using FEA

Plasticity effect on crack closure was regarded as a minor effect and was therefore not used in the model, not only because this simplified the model, but also because it did not affect the final results. In the regions of compressive residual stresses crack closure could occur causing an overlap of the crack. Nussbaumer [21] used gap elements to over come this issue. Dexter and Pilarski [6] did a case study on the use, versus non-use of gap elements. They reported that using gap elements introduces geometric non-linearity, which conflicts with the use of LEFM. They also found that using gap elements yields similar results as if they were not used. Furthermore, K_{res} derived from a gap element analysis is a little higher than the K_{res} when gap elements are not used. In other words, when gap elements are not used, ΔK_{eff} is high, resulting in a more conservative solution.

4.6   FE Model Predictions

For the first specimen (S1), two different scenarios were investigated. First, analysis was done by propagating the crack up to a certain distance in the stiffener's web, as was observed in the actual experiment.   In the first analysis, three different values of compressive residual stresses were used to investigate the propagation of the crack.

The second analysis was done by totally severing the stiffeners (i.e. crack propagates up the web and into the flange of the stiffener), which is a typical behavior observed in a ship. Fortunately, as could be seen in Figure 4-7, the crack propagation rate in the plate was not largely affected by severing the stiffeners. The reason for that is believed to be that the stiffeners were not effective in carrying the load. This observation was discussed in the experimental results section.
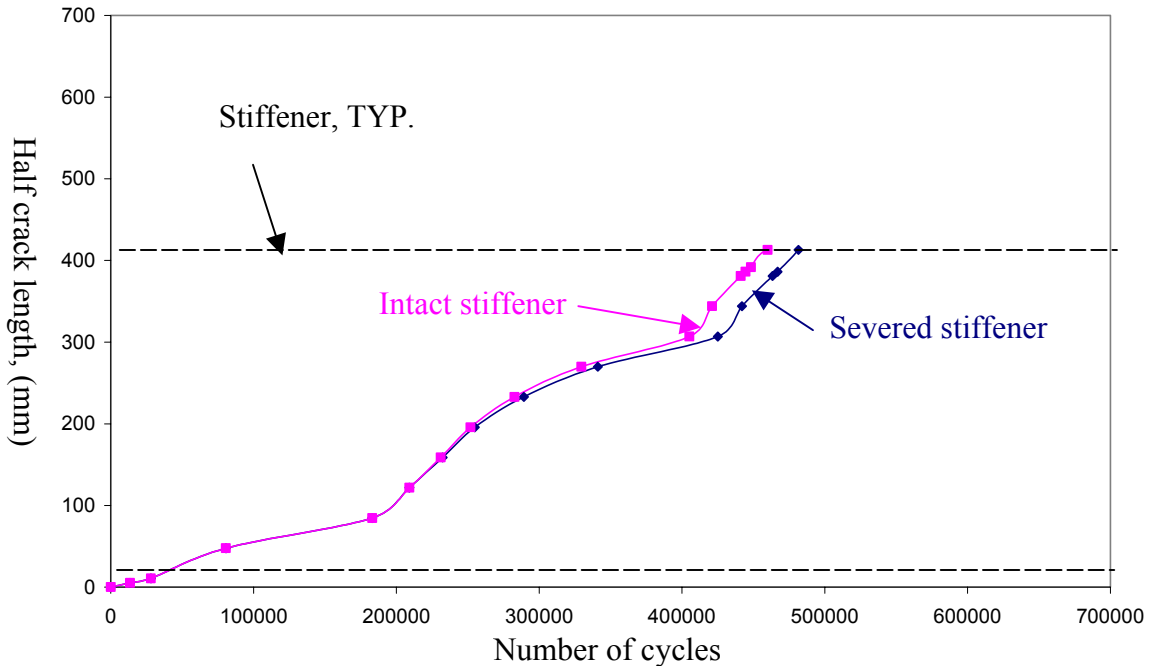
Figure 4-7 Finite element crack extension comparison between intact and severed stiffener

4.7   Comparison between Finite Element and Experimental Results

The finite element results varied based on the values used for the Paris equation parameter C, as well as the magnitude of the residual stresses. The C value of 9.5E-12 seemed to be an appropriate value to use for representing the actual propagation rate in the plate, keeping in mind that the proper value of compressive residual stresses is also used in the analysis. In the analysis of S1 the C value of 6.8E-12 appeared to be a non-conservative value and was therefore not used in the analysis of S2 - S5. A value of 1.68E-11 for C is adopted by the British Standards BS 7910. This value seemed to produce very conservative results, and in some cases underestimated the life by a factor of two. *(The above mentioned values of the parameter C are for units of MPa and m.)*

4.7.1 Specimen S1

Looking at Figure 4-8, one could see that using the compressive stress value of 100 MPa with a C value of 9.5E-12 results in fairly good agreement between the finite element analysis and the experimental results. The figure also shows that using a C value of 1.68E-11 underestimates the actual behavior and is excessively conservative. The result from using this value is very close to the result for a center crack tension panel (CCT) with a C value of 9.5E-12, which is a plate with no attached stiffeners. It is important to mention that as the value of the compressive residual stress decreases, the result using the C value of 1.68E-11 worsens. In other words, none of the three values used to represent the compressive residual stresses resulted in the finite element analysis being in an agreement with the experimental results when 1.68E-11 was used for C. As mentioned before, the C value of 6.8E-12 appeared to be non-conservative and was not further investigated for the remaining specimens.

58
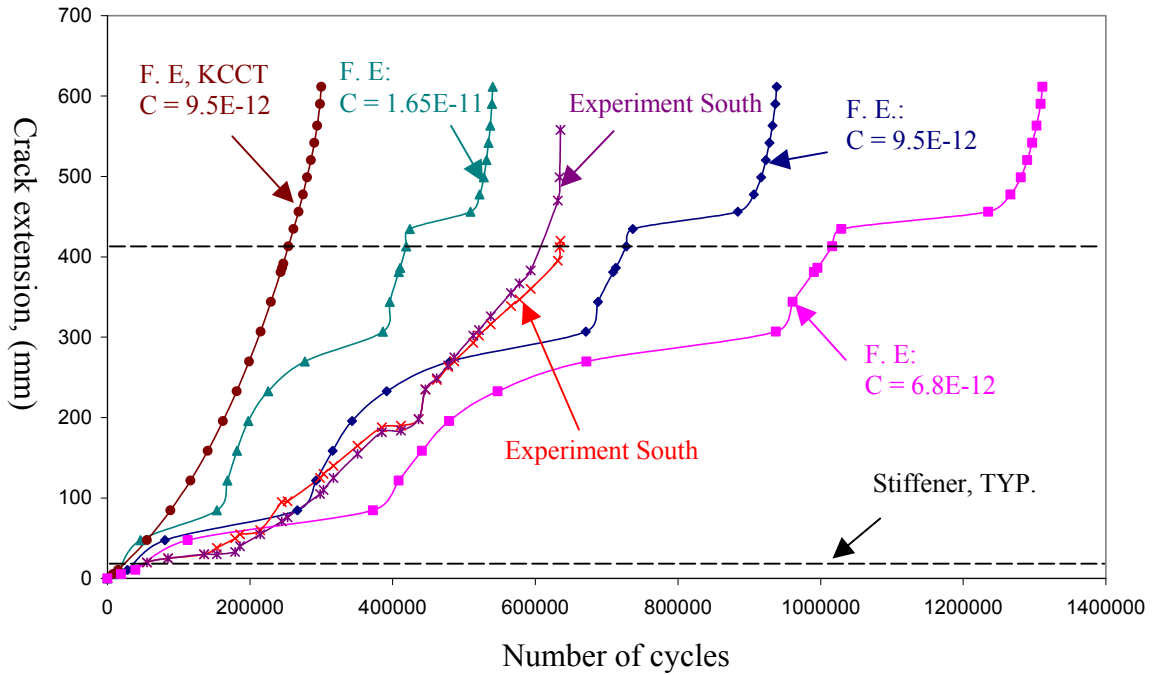
Figure 4-8 Crack extension versus cycles for comp. residual stresses of 100 MPa

As discussed above, because of the scatter in the measurements of residual stresses, the finite element analysis was done using three different values of compressive residual stresses to investigate the effect of the magnitude on the propagation rate, and to determine which value would best represent the actual value in the plate. Figure 4-9 shows the sensitivity of the results to the value of the stresses used. It also shows that using compressive stress value of 100 MPa was the most appropriate for the analysis.
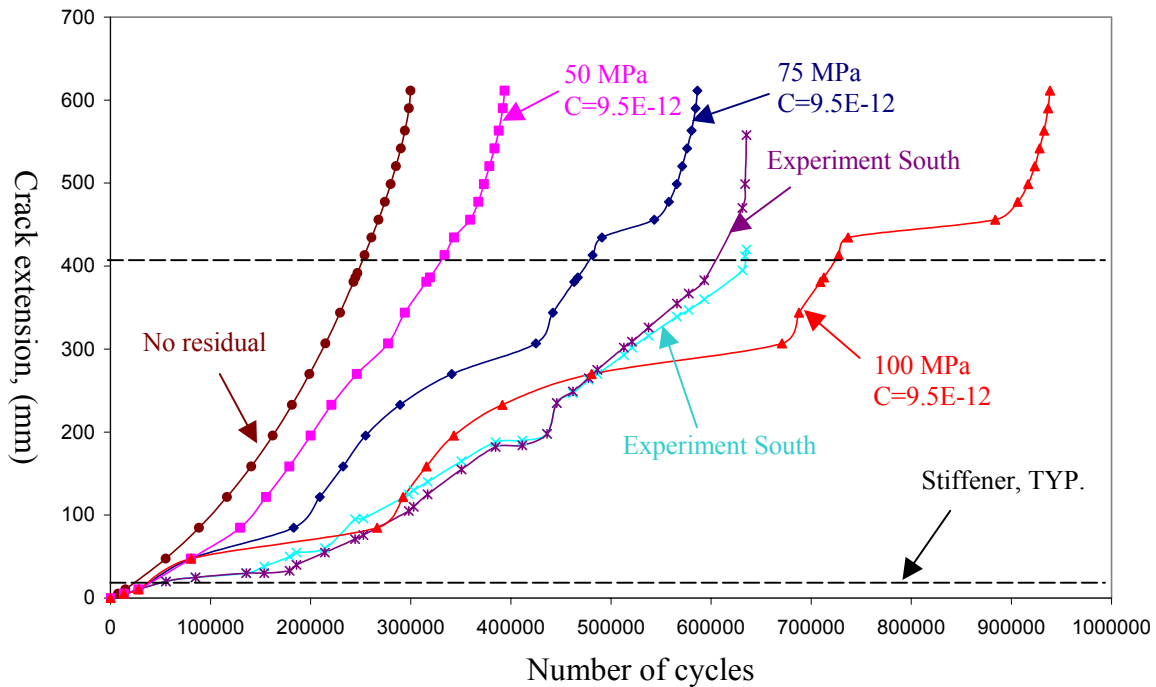
Figure 4-9 Crack extension versus cycles using compressive values of 50, 75, and 100 MPa

4.7.2 Specimen S2

As previously reported, a 20% difference in the propagation rate was observed when comparing specimen S1 and specimen S2. It is believed that the difference in the results was due to the different magnitude of the heat input used in the welding process. Even though high heat input was used to weld the stiffeners to the plate for specimen S2, it took fewer cycles to fail the specimen, which indicated a smaller magnitude of residual stresses in S2. As previously said, it is possible that during manufacture the specimens were marked incorrectly, where S1 was supposed to be marked as S2, and vice versa. Again, three different values of compressive residual stresses were investigated, as well as the two different C values.

The finite element results from specimen S1 were used for the comparison to the experimental results for S2.

Figure 4-10, and Figure 4-11 show that the most appropriate value for the magnitude of the compressive residual stresses is 75 MPa. It also shows that using the C value of 9.5E-12 is more appropriate than using a value of 1.68E-12.
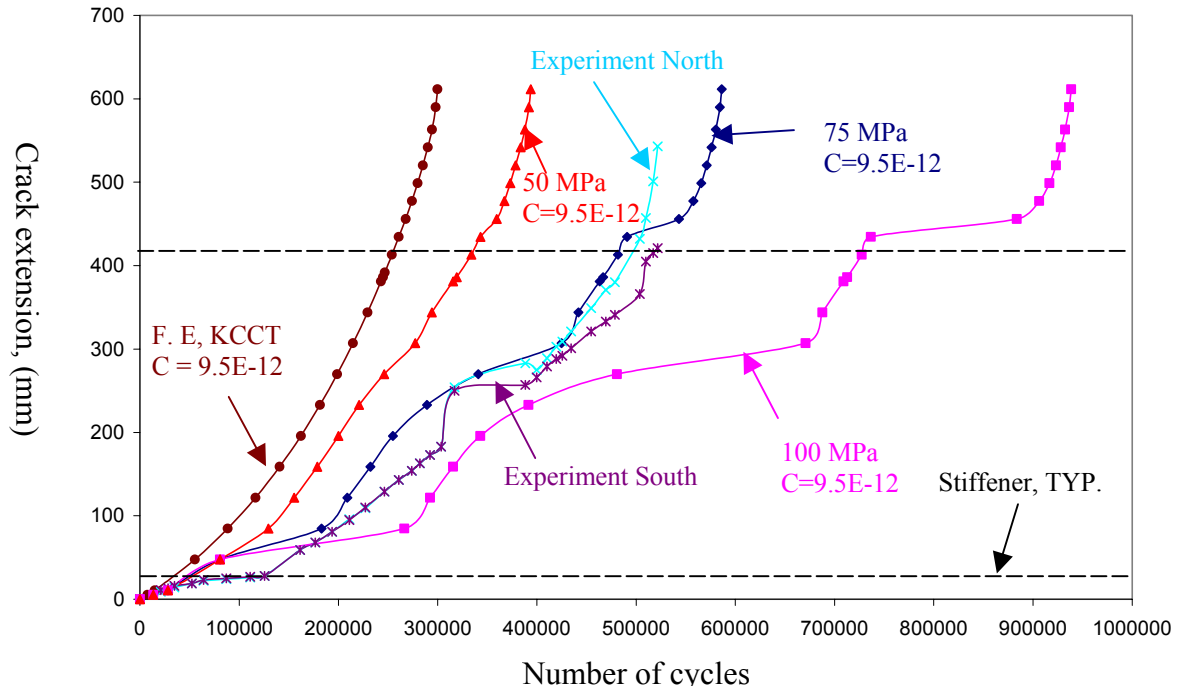
Figure 4-10 Crack extension versus cycles using comp. residual stresses of 50, 75, and 100 MPa
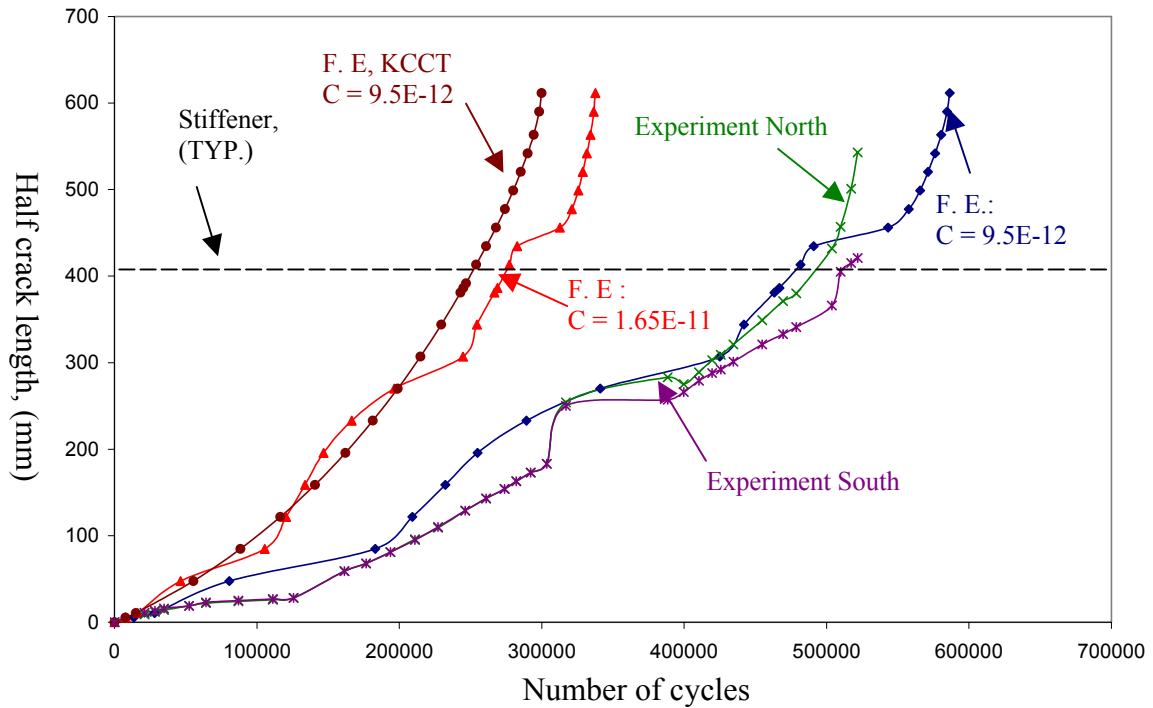
Figure 4-11 Crack extension versus cycles using comp. residual stresses of 75 MPa

4.7.3 Specimen S3

An increase in the magnitude of the compressive residual stresses was predicted since the spacing between the stiffeners for specimen S3 was smaller than the spacing in S2. It is believed that the compressive residual stress in S3 was of higher magnitude than that of S2 as specimen S3 experienced approximately 25,000 more cycles to failure than specimen S2. The experiment as well as the finite element indicates that average compressive residual stresses of 100 MPa existed in the plate considering that the C value of 9.5E-12 is an appropriate value to use in the Paris Law to determine the crack propagation rate. It is also clear that the magnitude of the compressive residual stress in specimen S3 is slightly higher than that of S1. In other words, reducing the spacing between the stiffeners was more effective in increasing the magnitude of compressive residual stresses than using higher heat input (assuming that S1 had high heat input, not S2).
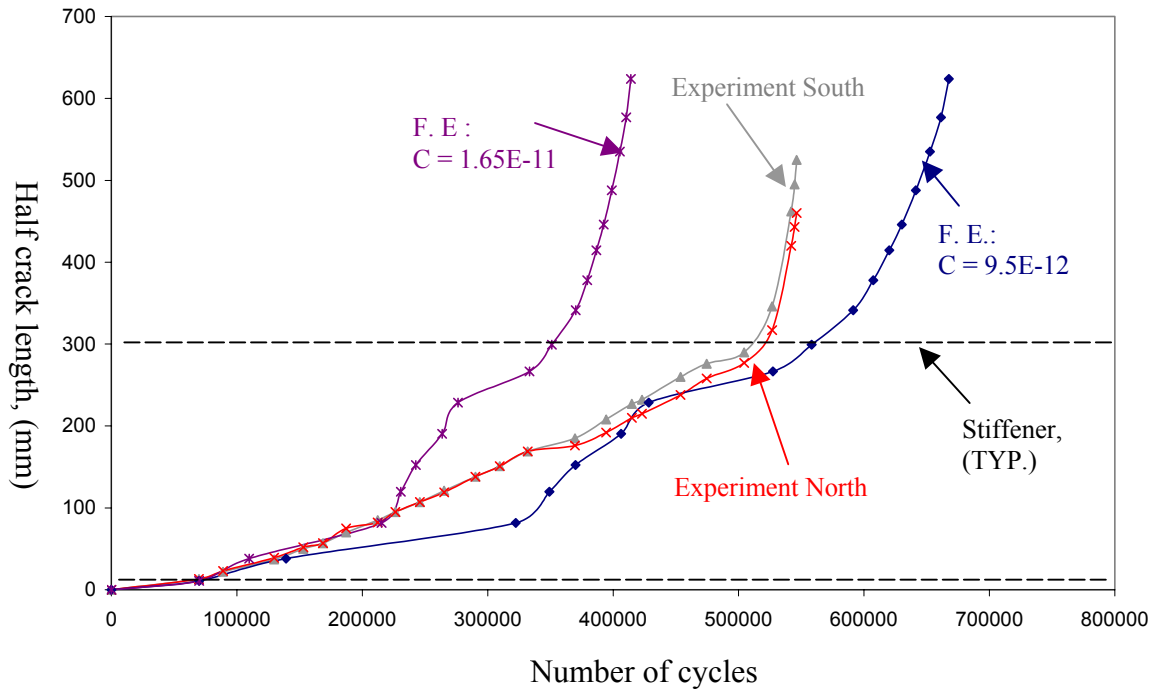
Figure 4-12 Crack extension versus cycles for comp. residual stresses of 100 MPa
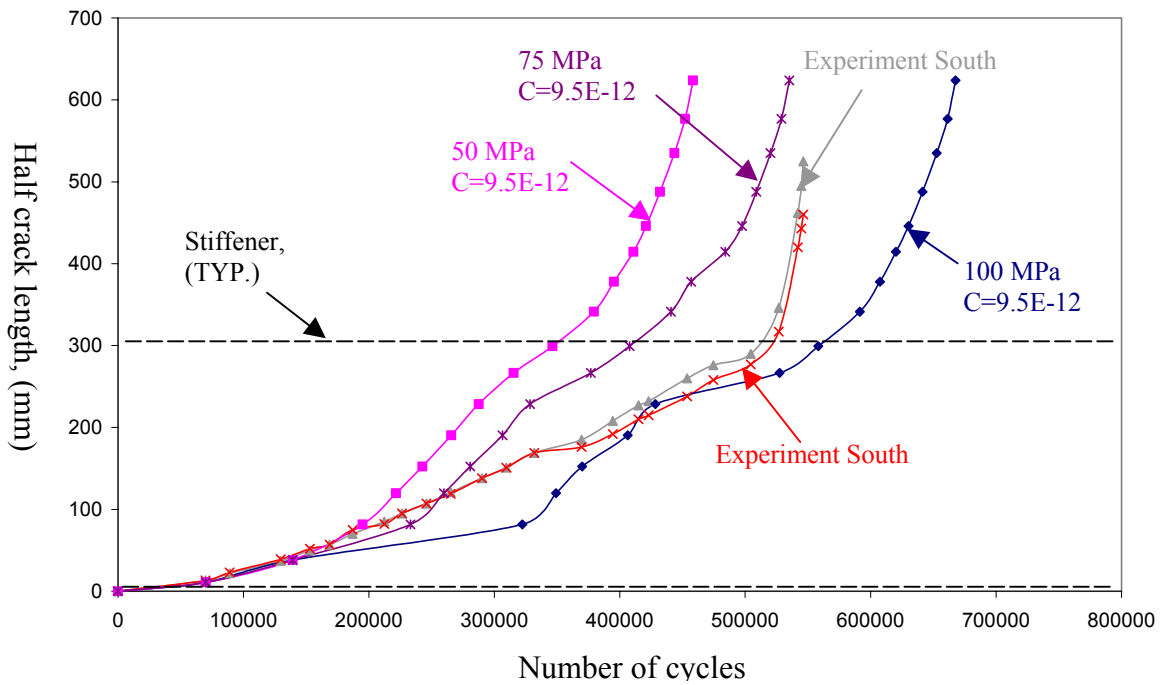
Figure 4-13 Crack extension versus cycles for comp. residual stresses of 50, 75, and 100 MPa

63

4.7.4　Specimen S4

The finite element analysis for specimen S4 showed that the computed values of $K_{app, max}$, and $K_{app, min}$, were very similar to those of the specimen with the same plate thickness and stiffeners spacing (S2). In fact, the values were identical between the stiffeners, and only slightly different next to the stiffeners. This small difference had a slight effect on the total number of cycles before the propagation became unstable. The slight difference in the propagation is believed to be attributed to the minor difference in the magnitude of the residual stresses between specimens S1 and S4.   However, this could not be confirmed since no measurements of residual stresses were taken in specimen S4.
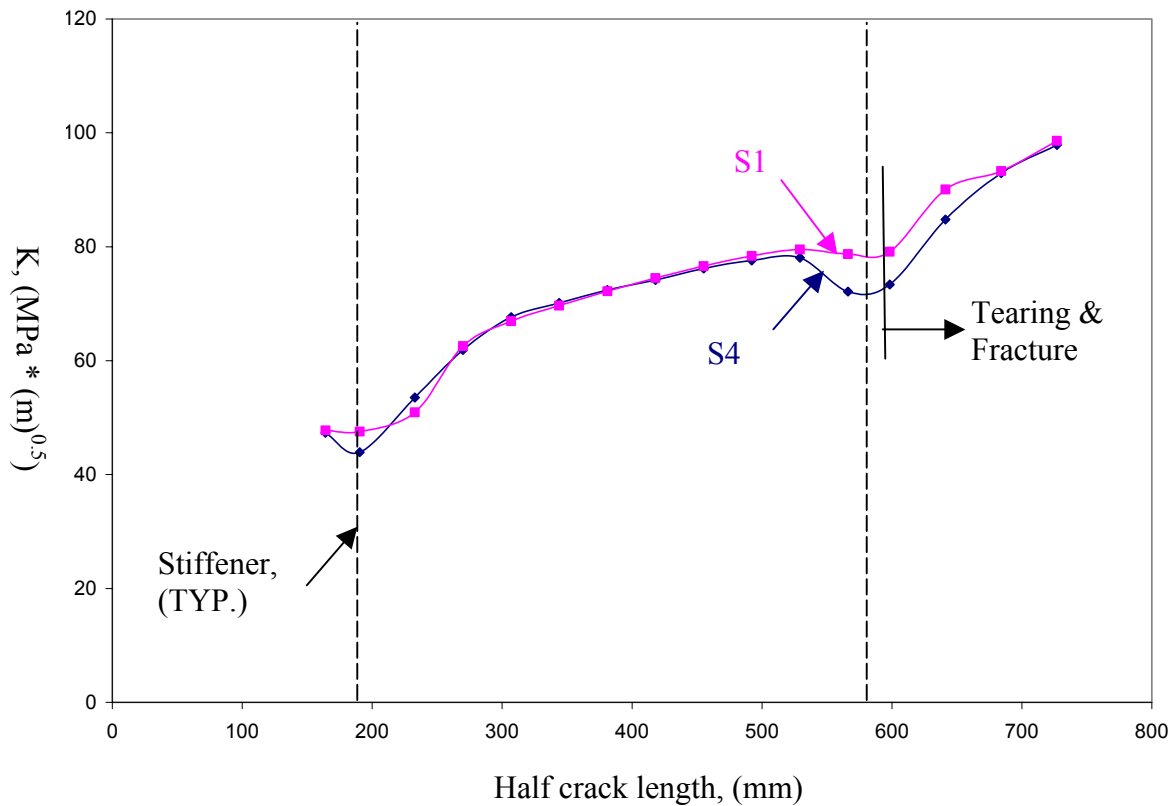
Figure 4-14 Comparison of K_{max} values between S1 & S4

4.7.5 Specimen S5

The geometry of specimen S5 was the same as that of S1 and S2, except that specimen S5 had a plate thickness of 9mm, while S1 and S2 had a 13 mm thick plate. A parametric study was done to investigate the effect of plate thickness on the values of the stress intensity factor K. Four different crack lengths were chosen across the stiffened panel. The J-integral values were calculated, and converted to K values. It was found that the calculated values of K are at maximum 1% higher than those values obtained from the analysis of specimen S1, which had a 13mm thick plate.

Because the small difference in plate thickness did not have much effect on the calculated K values, it was of interest to investigate the effect of the ratio of the stiffness of the stiffeners to the stiffness of the plate with the stiffeners added together, also known as μ on the calculated K value.

For the given stiffeners and plate geometry the μ value is 0.26, which is a typical value found in a ship structure. A parametric study was done where the area of the stiffeners was doubled giving a μ value of 0.41. It was found that the calculated K values were at maximum 3% less than those where μ was equal to 0.26. The reason for this is that the tensile force was only applied to the plate, thus the stiffeners did not carry a significant portion of the load. This could also be seen in Figure 4-15 where the value of K/K_{CCT} is always close to one, except when the K value was calculated close to the stiffener. This indicates that next to the stiffeners the K values drop down, but as the crack propagates past the stiffeners the K values stays the same whether there are stiffeners or not.
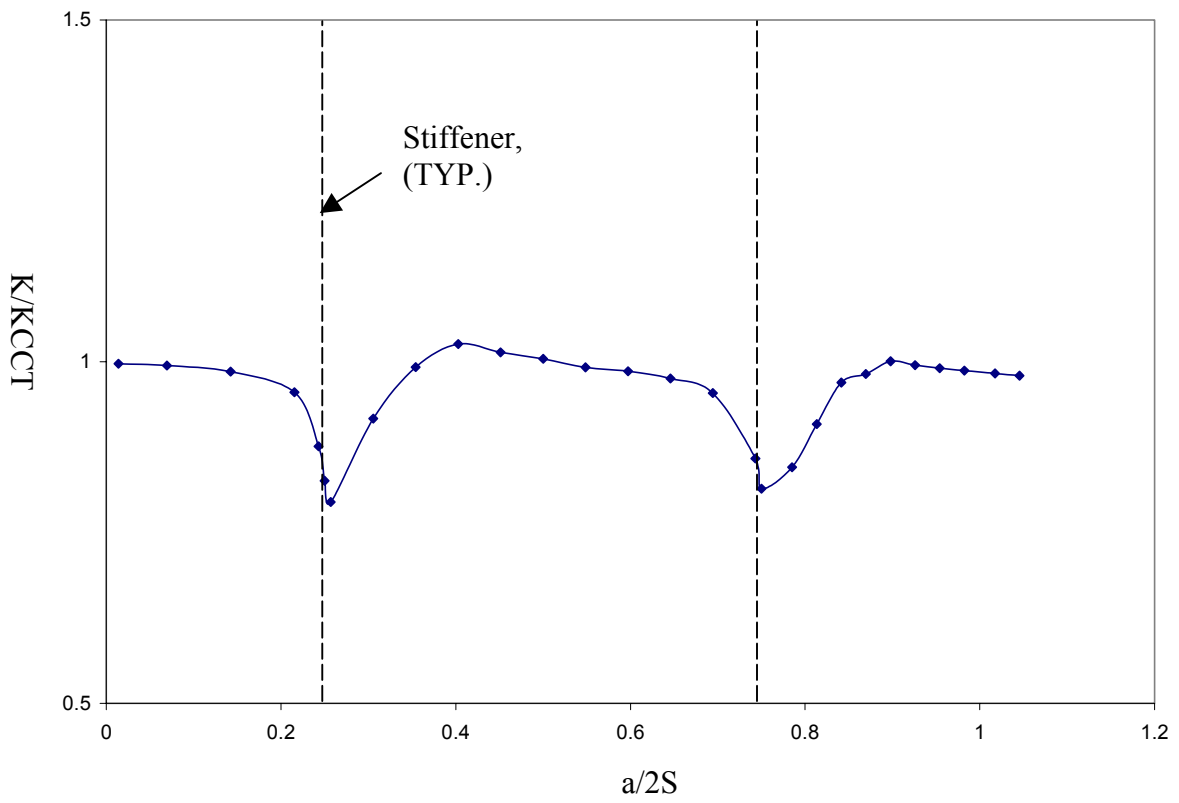
Figure 4-15 K/K$_{CCT}$ for specimen S1

5   CONCLUSION

Five experiments were conducted to investigate fatigue crack propagation in welded stiffened panels, which are typical of ship structures. The specimens varied in the spacing, geometry, and heat input used for welding of the stiffeners.

Linear-elastic finite-element models of the specimens were developed to calculate the range in the stress intensity factor, which was then used to estimate the crack propagation rate. Residual stresses were incorporated in the model as initial stresses. The model was validated by comparing the calculated crack propagation with the experimental results.

The following conclusions were reached:

1.   The crack propagation remained stable despite crack lengths up to 750 mm and peak stress of 70 MPa.

2.   There is a substantial reduction in the crack propagation rate in stiffened plates relative to what would be expected in a plate without stiffeners. The cycles to propagate one stiffener spacing may increase by a factor of 2 to 4 above what would be predicted for a center-cracked plate.

3.   Crack propagation rate in the these specimens was similar to the propagation rate observed in highly redundant box sections loaded in bending tested in a previous project, suggesting that redundancy and stress gradient in the box section tested previously had little effect on the propagation rate.

4.   Two factors cause the reduction in the crack propagation rate in a stiffened panel: the restraint effect and the compressive residual stress between stiffeners arising from the welding process. These two factors are about equally important in these experiments.

5. Measured residual stress showed high variability in magnitude with a consistent pattern of tensile residual stress adjacent to the stiffeners and compressive residual stress between the stiffeners. The pattern is consistent with past studies of residual stress in welded stiffened panels.

6. The spacing of the stiffeners has an obvious effect on the reduction in crack propagation rate as well as the overall number of cycles to failure. The magnitude of the compressive residual stresses increases as the spacing between the stiffeners decreases.

7. The crack propagation rate up in the stiffener's web has the same rate as it continues to propagate in the plate pass the stiffener

8. The analysis using the finite element method to calculate the range in stress intensity factor, followed by using Paris's Law to predict the crack propagation, gave good agreement with the experiments provided that reasonable values for the parameters of the crack growth rate equation were chosen.

9. Simple spreadsheet analysis gave as good agreement with the experimental data as the finite-element analyses at much lower effort. It is recommended that no finite-width correction be used with this analytical model.

6   RECOMMENDATION

The experiment, along with finite element analysis, showed the sensitivity of the results for crack propagation rate to the magnitude of residual stresses as well as the C value chosen for the Paris Law equation. The scatter in the measured values in the residual stresses suggests the following:

1. The statistical variation in compressive residual stress between stiffeners should be quantified, including the effect of welding procedure and welding sequence.

2. There is great variability in fatigue crack growth and the loading; therefore accurate predictions are not possible. However, reasonable "upper-bound" models, such as developed in this research, can be used to confidently predict the crack propagation in stiffened panels.

7   REFERENCES

1.   www.imo.org/newsroom/mainframe.asp?topic_id=72

2.   Dexter, R.J., and M.L. Gentilcore, "Evaluation of Ductile Fracture Models for Ship Structural Details", Report SSC-393, Ship Structure Committee, Washington, D.C., 1997.

3.   Tanker Structure Co-operative Forum. Int'l Chamber of Shipping and Oil Companies Int'l Marine Forum. "Guidelines for the Inspection and Maintenance of Double Hull Tanker Structures". London, England: Witherby & Co., Ltd, 1995.

4.   Tanker Structure Co-operative Forum. Int'l Chamber of Shipping and Oil Companies Int'l Marine Forum. "Guidance Manual for the Inspection and Condition Assessment of Tanker Structures". London, England: Witherby & Co., Ltd., 1986.

5.   R. J. Dexter, P. J. Pilarski "Crack Propagation in Welded Stiffened Panels" Journal of Constructional Steel, Vol. 58, pp. 1081-1102, 2002.

6.   R. J. Dexter, P. J. Pilarski, "Effect of Welded Stiffeners on Fatigue Crack Growth Rate", Ship Structure Committee Report (SSC 413), NTIS#: PB00-108445, August 2000.

7.   N. E. Dowling, Mechanics Behavior of Materials, (2nd ed.) Prentice hall, Upper Saddle River, New Jersey, 1998.

8.   T. L. Anderson, Fracture Mechanics, (2nd ed.) CRC Press LLC, Boca Raton, Florida, 1995.

9.   Rushton, P. A., "An Experimental And Numerical Investigation Into Fatigue Crack Propagation of 350 WT Steel Subjected to semi-Random cyclic Loading, DREA CR 2000-154, March 2001.

10.   P. Paris, F. Erdogan. "A Critical Analysis of crack Propagation Laws". Trans. ASME, Ser. D. Journal of Basic Engineering, Vol.85, N 4, pp. 528-534, 1963.

11.   Kober, R. J. Dexter, B. T. Yen, J. W. Fisher, "The Effect of Welding Discontinuities on the Variability of Fatigue Life", Fracture Mechanics, Vol. 25.

12.   Barsom J. M. and s. T. Rolfe "Fracture and Fatigue Control in Structures" 2nd ed. Englewood Cliffs, New Jersey: Prentic Hall, 1987.

13.   BS 7910:1999 "Guide on Methods for Assessing the Acceptability of Flaws in Metallic Structures". British Standards Institute, London, 1999.

14.   Fisher, J.W., et al. Phase I: Final Report—"Development of Advanced Double Hull Concepts", Vol.3a, Structural Failure Modes: Fatigue, Final Report for Cooperative Agreement N00014-91-CA-0001, Lehigh University, Bethlehem, PA, March 1993.

15.   BS6493: 1993 "Fatigue Design and Assessment for Steel Structures".

16.   C. Poe "The Effect of Riveted and Uniformly Spaced Stringers on The Stress Intensity Factor of a cracked Sheet", Master of Science dissertation, 1969, Virginia: Virginia Polytechnic Institute.

17.   C. C. Poe, "Fatigue Crack Propagation in Stiffened panels", Damage Tolerance in Aircraft Structures, ASTM STP 486, American Society for Testing and Materials, pp. 79-97, 1971.

18.   Thayamballi Mathummal, Anil Kumar. "Reliability of Ship Hull in the Fracture and Fatigue Modes of Failure." Ph.D. dissertation in Engineering. 1983. University of California, Berkeley.

19.   D. Faulkner, "A Review of Effective Plating for use in the Analysis of Stiffened Plating in Bending And Compression" Journal of Ship Research, Vol. 19, 1975, pp. 1-17.

20.   H. Petershagen, W. Fricke "Fatigue Crack Propagation in Plate Panels with Welded Stiffeners". IIW-Doc. XIII-1272-88. Technical University of Hamburg, 1988.

21.   A. Nussbaumer "Propagation of Long Fatigue Cracks in Multi-Cellular Box Beams" Ph.D. dissertation in Civil Engineering, 1993. Bethlehem, Pennsylvania: Lehigh University.

22.   Weicheng et. al., "Strength of Ship Plates Under Combined Loading", Marine Structures Vol 15, pp. 75-97, 2002.

23.   Osgood, William R. "Residual Stresses in Metals and Metal Construction". New York: Reinhold Publishing Corp. Prepared for the Ship Structure Committee, 1954.

24.   M. E. Fitzpatrick, L. Edwards, "Fatigue Crack/Residual Stress Field Interactions and Their Implications for Damage Tolerance Design." JMEPEG, Vol. 7, pp. 90-98, 1998.

25.   J. Lu, handbook of Measurements of Residual Stresses, Society For Experimental Mechanics, INC. pp. 228-230, 1996.

26.   Beghini, M., L. Bertini and E. Vitale. "Fatigue Crack Growth in Residual Stress Fields: Experimental Results and Modeling." Fatigue and Fracture of Engineering Materials, Vol. 17, N 12, pp. 1433-1444, 1994.

27.   P. Pilariski "Effect of Welded Stiffeners on Crack Growth Rate" Masters of Science dissertation, 1999, Minneapolis, Minnesota: University of Minnesota.

28.   W. Elber "Fatigue Crack Closure under Cyclic Tension." Engineering Fracture Mechanics, Vol, 2, 1970. pp. 37-40.

29.   "Standard Specification for Structural Steel Ships", Designation: A131/A 131M-01, August, 2001.

30.   J.R. Rice "A PATH independent Integral and the Approximate Analysis of Strain Concentration by Notches and Cracks." Journal of Applied Mechanics, Vol. 35, pp. 379-386, 1986.

31.   R. D. Cook, et.al, "Concepts and Applications Of Finite Element Analysis", (3rd ed.) John Wiley & Sons, 1989.

32.   R.D. C, K.G. Shaw, "Crack Tip Finite Elements in Linear Fracture Mechanics" International Journal for Numerical Methods in Engineering, Vol. 9, pp. 495-507, 1975.

33.   R.S. Barsoum "On the Use of Isoparametric Finite Elements in Linear Fracture Mechanics" International Journal for Numerical Methods in Engineering, Vol. 10, pp.25-37, 1976.

8   APPENDIX A: Test Frame Cracking and Repair Method

8.1   Introduction

The frame used for the test program experienced problems during the actual testing. The problems varied from bolts failing, to cracking of members and welds. The cracks in the frame needed to be repaired to ensure the continuation of the test program. Even though repairing cracks is beyond the scope of this project, it is believed that valuable data from the failures was obtained and that the reporting of this data might be of help or use in future research.

8.2   Bolts Failure

Some of the bolts connecting the angles to the top and bottom beams were failing by fatigue. The bolts started to fail after approximately 150,000 cycles. Under-calculation of the stresses seen by the bolts was the reason for the failure. An air impact gun was used to pretension the new bolts without having to stop the actual testing. C-clamps were used as a way of reducing the stresses seen by the bolts.

Figure 8-1 shows the angel connecting the specimens to the top beams. Every angle is connected to the four beams W 27 x 84 by bolts (2 per beam). The total number of bolts for each angel is 8. To be able to distinguish between the different bolts, the first bolt is numbered "bolt # 1" as shown in Figure 8-1. The remaining bolts are numbered in order, so the last bolt is "bolt # 8". Tables 6-1 to 6-4 show the bolt number versus the number of cycles it took until failure.
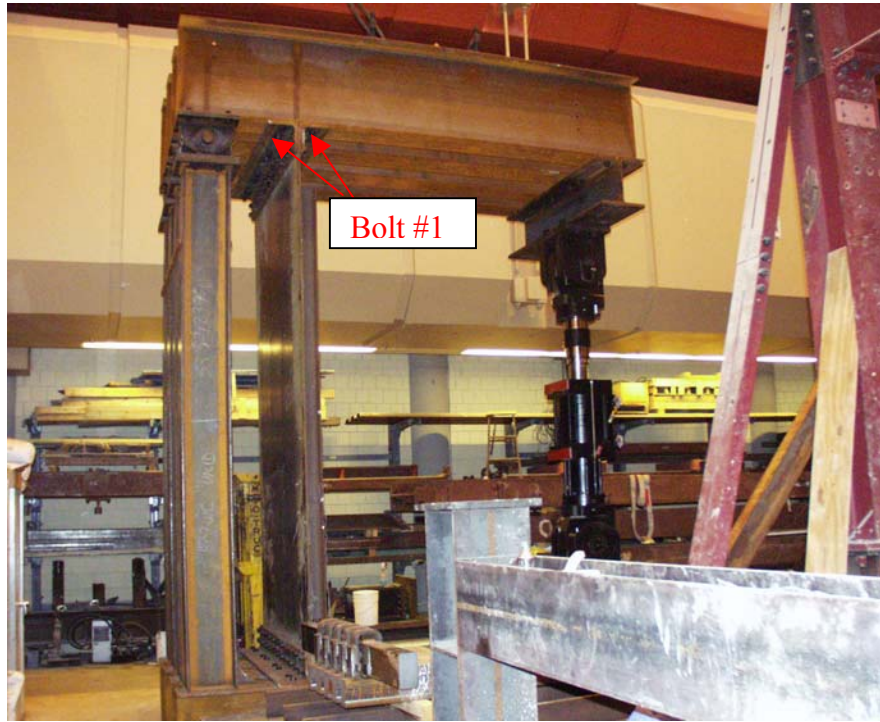
Figure 8-1 Side view of test frame showing the angle to beam connection
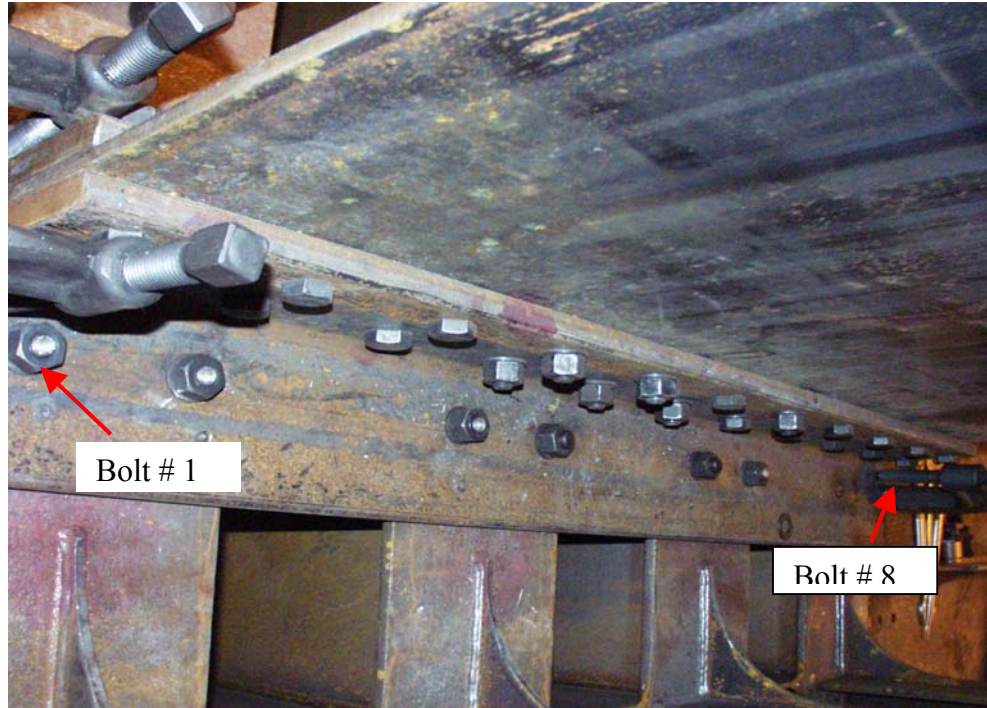
Figure 8-2 Angle to beam connection

The stresses seen by each bolt are as follows:-

Maximum load applied to bolts = 333.5

$$p = \frac{333.5^k}{16} = 20.84 \text{ k / bolt}$$

Tensile stress area " TSA " = 75% of nominal area = 0.75 * 0.601 = 0.45 in^2

$$\Delta F_{bolt} = \frac{20.84^k}{0.45 \text{ in}^2} = 46.3 \text{ ksi}$$

Using 20 % rule = 0.20 * ΔF_{bolt} = 0.2 * 46.3 = 9.26 ksi

- All bolts are 7/8" x 3" A-325 structural steel bolts
- Bolts were replaced immediately after failure was discovered

Table 8-1 Bottom left bolt's number and the number of cycles to failure

Bolt number	Number of cycles
1	154,000
5,6	$180,000 \pm 10,000$
3,4	$200,000 \pm 10,000$
2	250,000
7	Never failed
8	Never failed

Table 8-2 Bottom right bolt's number and the number of cycles to failure

Bolt number	Number of cycles
3,4	210,000
1,2	$220,000 \pm 10,000$
5	$240,000 \pm 10,000$
6	250,000
7,8	265,000

Table 8-3 Top left bolt's number and the number of cycles to failure

Bolt number	Number of cycles
4	240,000
7,8	$260,000 \pm 10,000$
1	280,000

Table 8-4 Top right bolt's number and the number of cycles to failure

Bolt number	Number of cycles
5,6	$190,000 \pm 10,000$
3	210,000
1	280,000

- At this point all bolts were replaced and clamps were added
- The average number of cycles to failure for bolts before adding clamps was about 250,000 cycles.
- The average number of cycles to failure for bolts after adding clamps was about 450,000 cycles.
- For bottom left, bolt # 8 was ¾" A490. It failed after about 2,000,000 cycles!
- The numbering of bolts from 1 to 8 is the same for all angles (8 being the last one going into the page).

The high stress experienced by the bolts placed the bolts under fatigue category E'. Figure 8-3 shows the S-N curve for the data of the failed bolts. All of the bolts are below the curve for category E'. After the C-clamps were added, the test resumed and the bolts were failing every approximately 400,000 cycles. Because of the high 3-D state of stress at the location where the angles are connected to the top and bottom beams, two new types of failures occurred. The first type was failure of the transverse weld connecting the diaphragms to the flanges of the W 27 x 84, and the second type was failure of the web/flange intersection of the w 27 x 84.
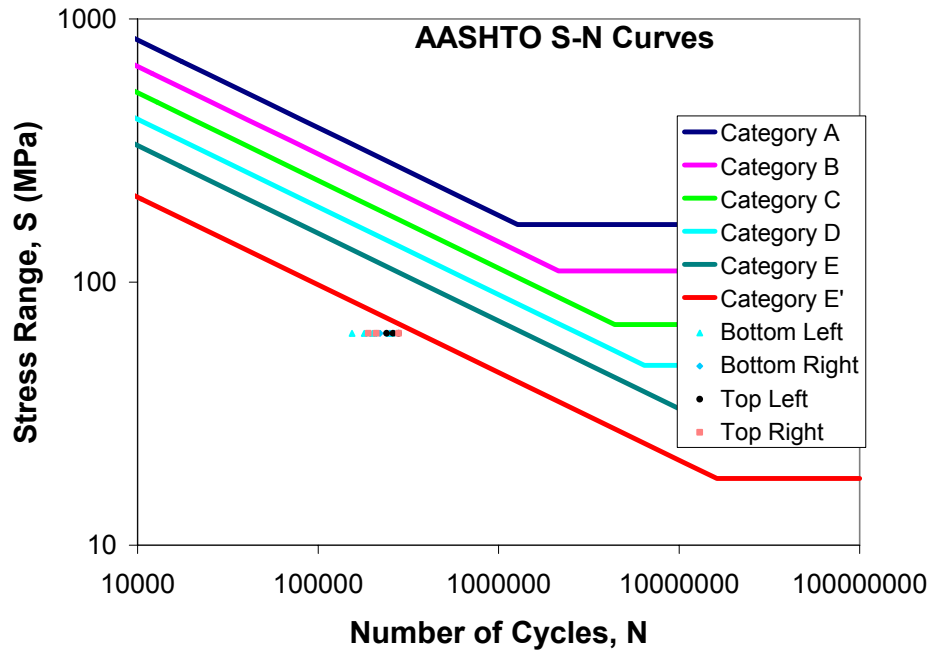
Figure 8-3 S-N curve for failed bolts

8.3   Transverse Weld Cracking

The problem of cracks in welds has been known by engineers for a long time. Generally speaking, tiny cracks are known to exist in welds even before the structure is in service. Micro cracks with an initial size of approximately 0.2 mm could grow longer in length as the welded detail experience fatigue cycles. The most common location of crack propagation is at the weld toe or the weld termination.

Figure 8-4 shows the diaphragm to beam connection with a through thickness crack in the transverse weld.
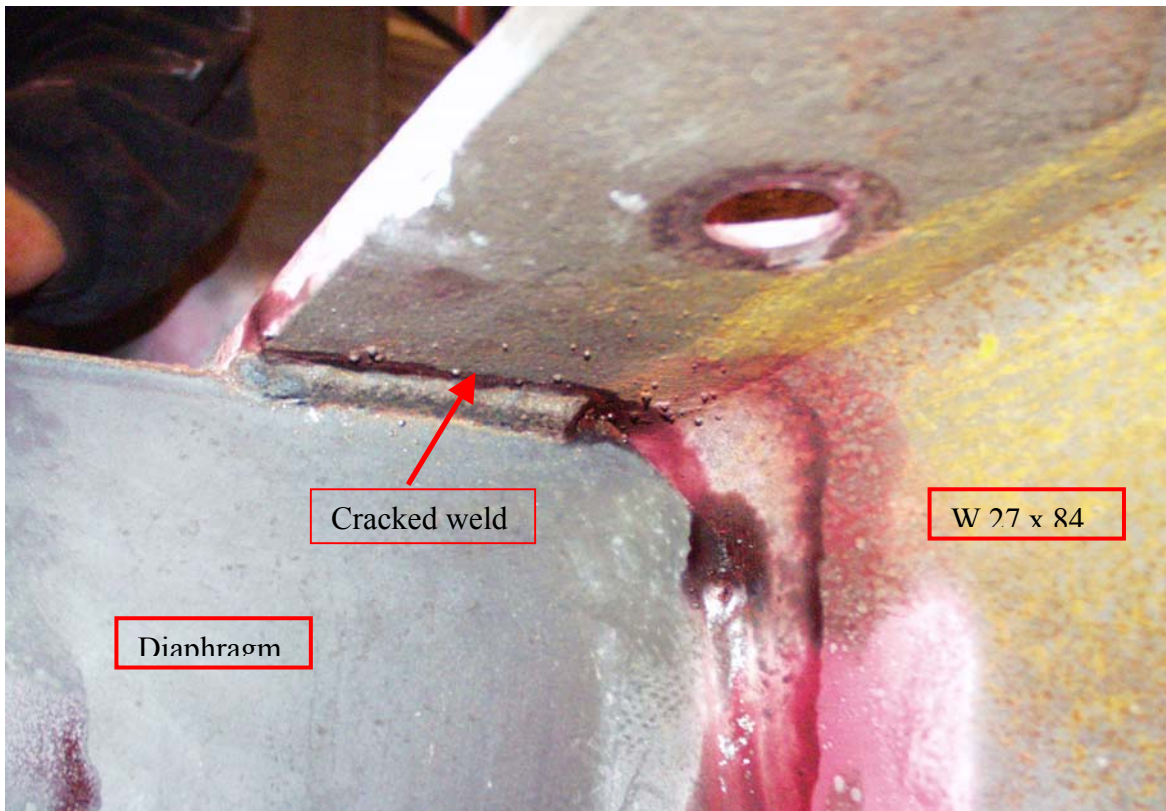
Figure 8-4 Through thickness crack in a transverse weld.

8.4 Web/Flange Cracking

Unfortunately, the problem of the bolt failure led to the welds cracking, which eventually led to cracking of the beam/flange intersection. The cracks in the top beams were very intensive and beyond repair. A replacement of the top beams was necessary for the continuation of the program. Two of the bottom beams experienced some cracks. The severity of the damage varied between the two beams, one experiencing much more damage than the other. Figure 8-5 shows one of the bottom beams with a crack 230 mm in length.
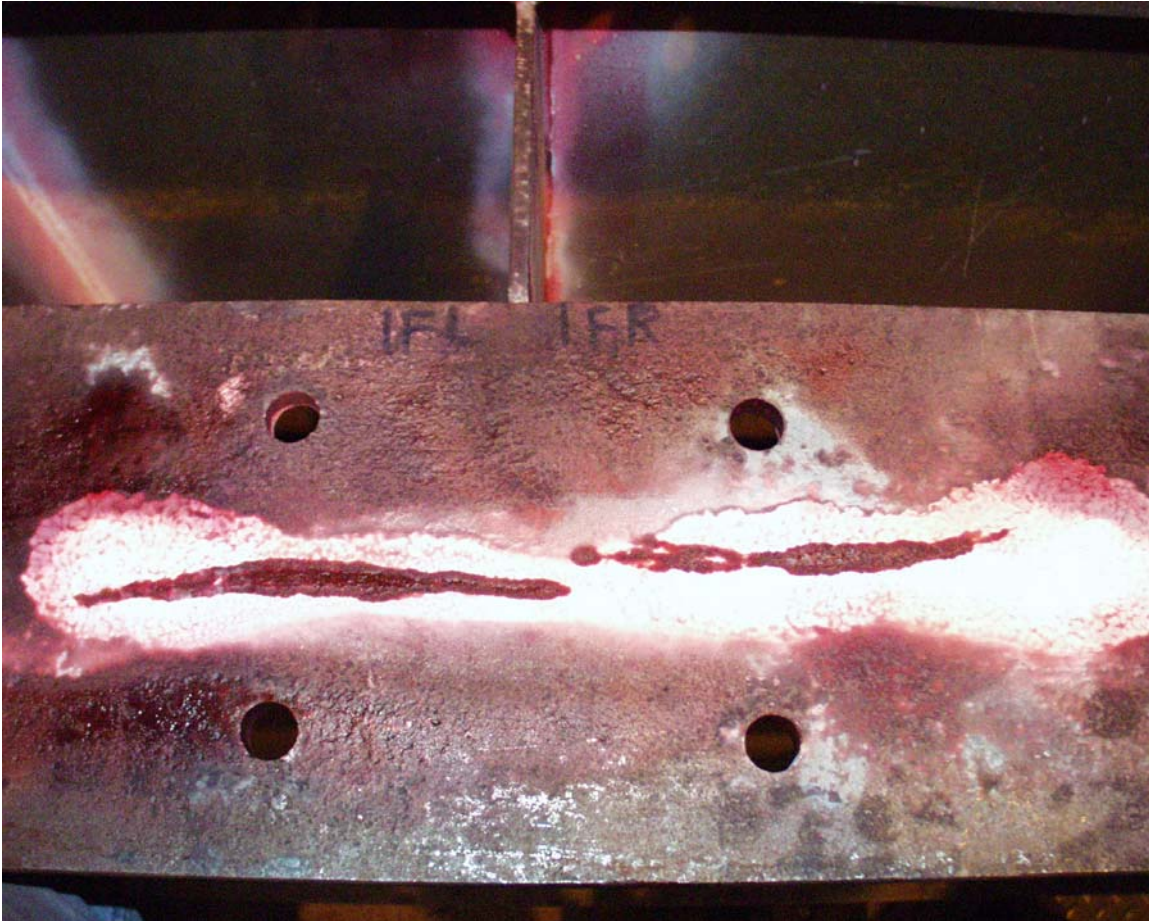
Figure 8-5 A through thickness crack at the flange/web intersection

8.5   Repair Method

Gouging out the cracked weld, and re-welding the diaphragms to the beam was the method used to repair the cracked weld. The gouging was done from both the top and the bottom of the diaphragms. Fillet weld was used to refill the gouged area. The weld was ground smooth at the top of the beam to allow angles to set perfectly horizontal on the beams. Hole drilling was used to arrest the cracks in the beams. The hole diameter was chosen to be approximately ¼ the crack length. In the case of the 230 mm crack, the hole was drilled as large as possible without losing too much of the section.
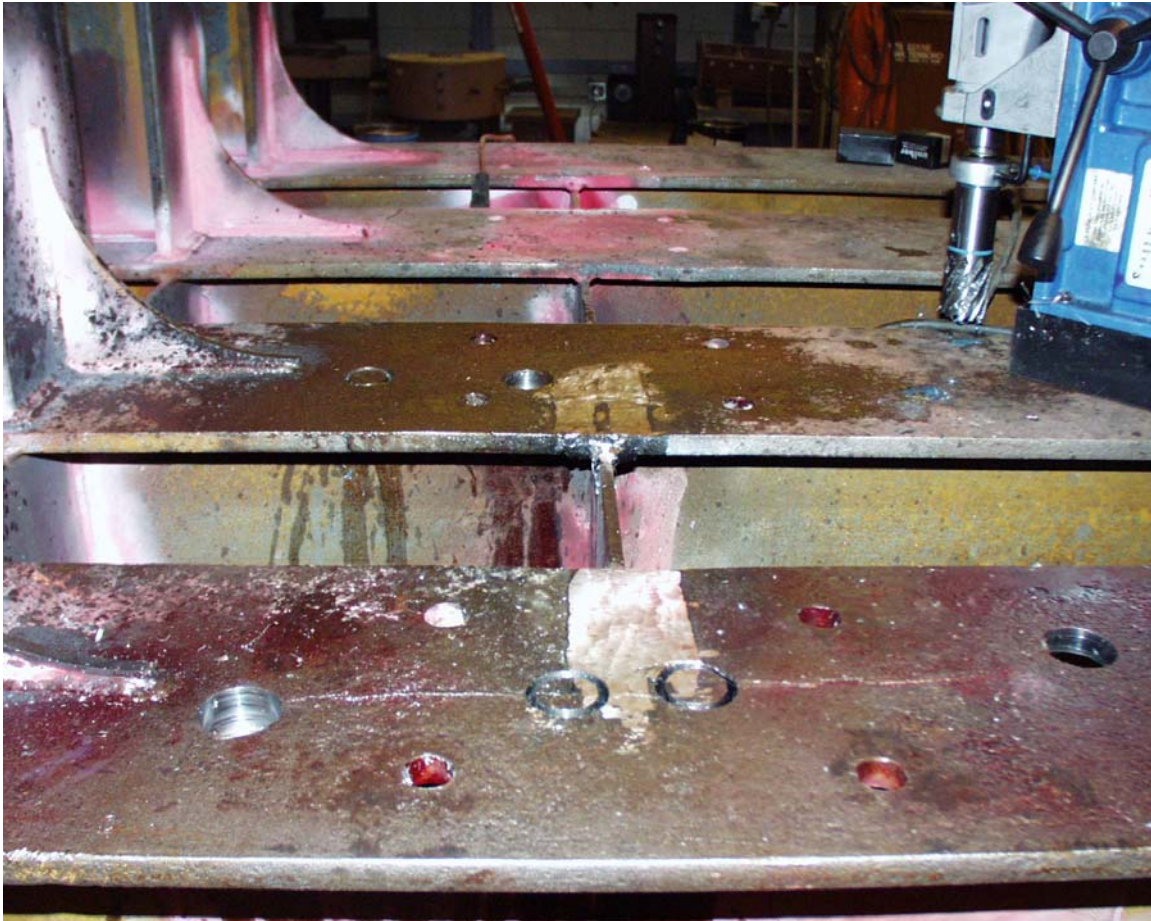
Figure 8-6 Weld ground smooth and holes drilled in beam

9 APPENDIX B: Analytical Model to Predict Crack Growth in Stiffened Panel

9.1 Analytical Spreadsheet Model Capabilities and User Instructions

An analytical model has been developed in Microsoft Excel to predict the growth of a fatigue crack in a steel panel. This program can be used for both stiffened and un-stiffened (CCT) panels. The Paris Law, as described in Section 2.6, is used to predict crack growth in the panel. The values of K and its modification factors for a stiffened panel can be found in SSC 413 [6]. It is assumed that the initial crack is centered on the panel and between stiffeners. It is also assumed that the stiffener spacing is constant across the panel.

To begin using the program, the user must input certain properties of the panel and the applied loading. These properties include the plate and stiffener geometry, number of stiffeners and spacing, and the minimum and maximum applied stress. Note that if a value of zero is entered for the number of stiffeners, the program will predict crack growth as for CCT. The user may then enter values for the initial and final crack length. If there is no initial crack, a value of zero must be entered for the initial crack length. The input of a final crack length is optional. If this input is left blank, the program will propagate the crack up to but not severing the final stiffener up to four stiffeners in each direction (a total of eight stiffeners across the panel). If a final crack length is entered, the crack will propagate this distance, assuming that it is not past the fourth stiffener, which is out of the range of the program's capabilities.

This program uses Faulkner's model for residual stress, as described in section 2.8. The user must specify the width of the tension block and the type of stress distribution, either a triangular or rectangular tensile residual stress block. Then, the user has the option of entering a maximum compressive residual stress. If this is done, the program will perform a force balance on the residual stress distribution and calculate the maximum tensile residual stress and the resulting distribution across the plate. If the maximum

compressive stress is not specified, it is assumed that the maximum tensile residual stress is equal to the yield stress of the plate, and again a balance of forces in the panel is used to determine the residual stress distribution. Should the user want to neglect the effects of residual stress in the propagation of the fatigue crack, the option of "None" should be chosen for the type of residual stress distribution.

The parameters of the Paris Law must also be specified. A discussion of these parameters can be found in section 2.6. It is recommended that for steel in air, the value of m be taken as 3.0, and the value of C is 9.5×10^{-12}. The crack growth increment, da, is also user specified. It is recommended that the value of da be small, on the order of 1 mm, in order to accurately capture the behavior of the fatigue crack propagation. However, the program is only capable of performing 1500 iterations, thus the crack growth increment cannot be smaller than 1500 times the desired crack extension, or the program will end before the crack reaches its desired final length. Also, the threshold ΔK must be entered. If the effective ΔK is less than the threshold ΔK at any point, the program will end and return a final crack length that is less than the desired extension.

A finite width correction as a modification factor for K can be used if desired. The user can specify either to use the secant formula or no finite width correction.

When the program is run, it will determine the number of cycles to failure for the stiffened panel and will also return the number of cycles to failure for an un-stiffened panel (CCT) with the same properties and initial crack length as the stiffened panel. If a value of zero is entered for the number of stiffeners, these two results will be identical. The program will display a plot of the number of cycles versus the crack length. Also, plots are created of the residual stress distribution, K_{res}, the applied and effective ΔK, and f_{st} versus the crack length.

9.2 Analytic Program Results

The results for crack propagation given by the analytic program are similar to those obtained using finite element analysis. When considering an un-stiffened steel panel (CCT) the analytic program closely predicts the results of the finite element analysis when no finite width correction factor is used, as shown below in Figure 9-1.
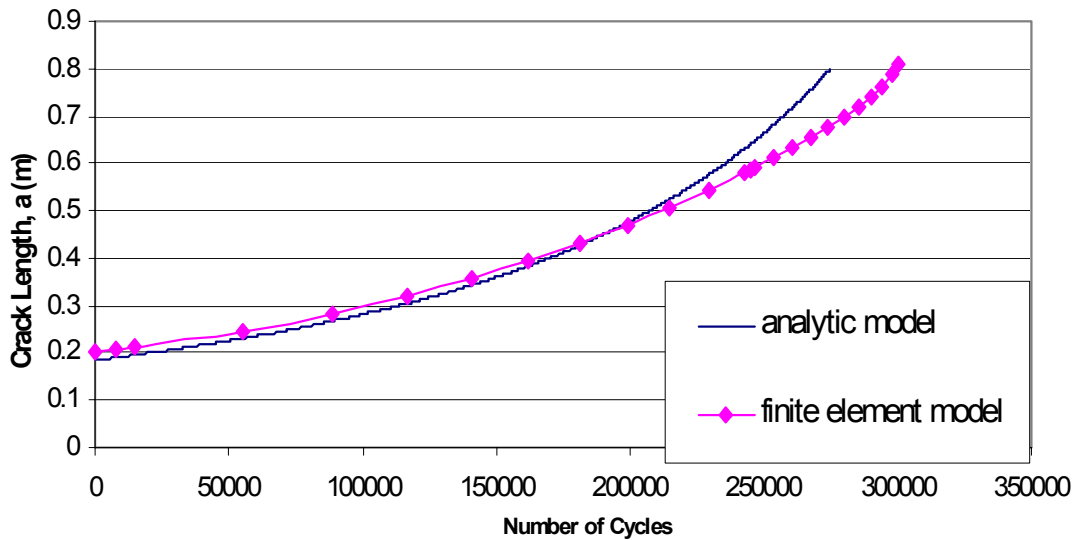
Comparison of CCT Crack Propagation Results for the Analytic Model versus the Finite Element Model

Figure 9-1 Comparison of CCT crack propagation results for analytic model versus finite element model

For a stiffened panel, the analytic program is sensitive to the type and magnitude of the residual stress distribution. With the finite-element model, reasonable but conservative results were obtained with the compressive residual stress equal to 75 MPa between stiffeners. Figure 9-2 shows the results of the analytical model for compressive residual stress of 75 MPa compared to the four experiments with the same stiffener spacing. Notice the very good agreement between the shape of the curves for the analytical model compared to shape of the experimental curves.
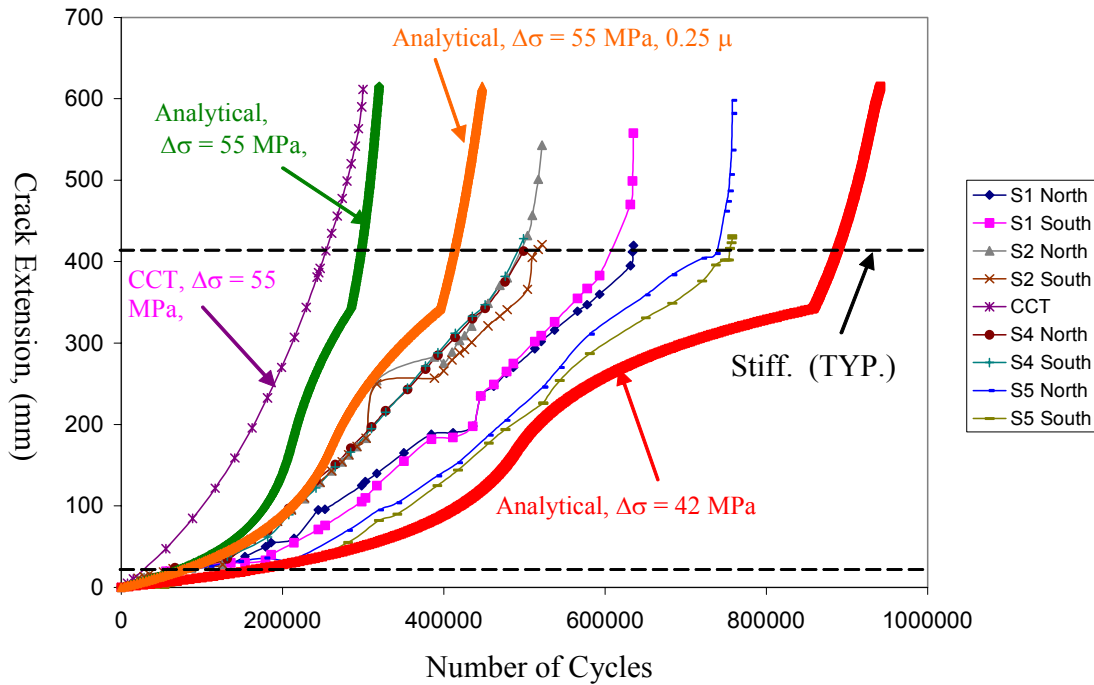
86

Figure 9-2 Comparison of experiments to Analytical Model with 75 MPa compressive residual stress between stiffeners with several applied stress range

The measured stress range in the plate in these tests was 55 MPa, however the stress was not uniform and the stress range in the stiffeners decreased with distance away from the plate but averaged less than 25% of 55 ksi. Therefore, when the model was run with 55 MPa as the stress range, the results are too conservative. The reason the results are too conservative is that the stiffener force, which is overestimated at 55 MPa, acts to increase stress-intensity factor from the splitting forces after the stiffener is severed.

The total load range divided by the cross-section area gives a stress range of 42 MPa. This is less than the 55 MPa because the 42 MPa is evenly distributed. When the analytical model was run with this lower stress range, the results are not conservative. This is because the stress range in the plate is much higher (55 MPa) in reality. As an attempt to model the shear lag in the stiffeners with the analytical model, the μ (stiffener to plate stiffness ratio) defined in Equation 2.7-1 was multiplied by 0.25, to reflect average stiffener stress range 25% of the stress range in the plate. As can be seen in

Figure 9-2, this case gives a reasonable and conservative upper-bound to the experimental data.

These same three analytical model results are compared to the finite-element analysis results for compressive residual stress equal to 75 MPa in Figure 9-3. The best agreement with this finite-element result is for the case that attempts to account for shear lag by reducing the stiffener force. It appears that the simple analytical model gives as good if not better agreement with the experiments than the finite-element analysis.
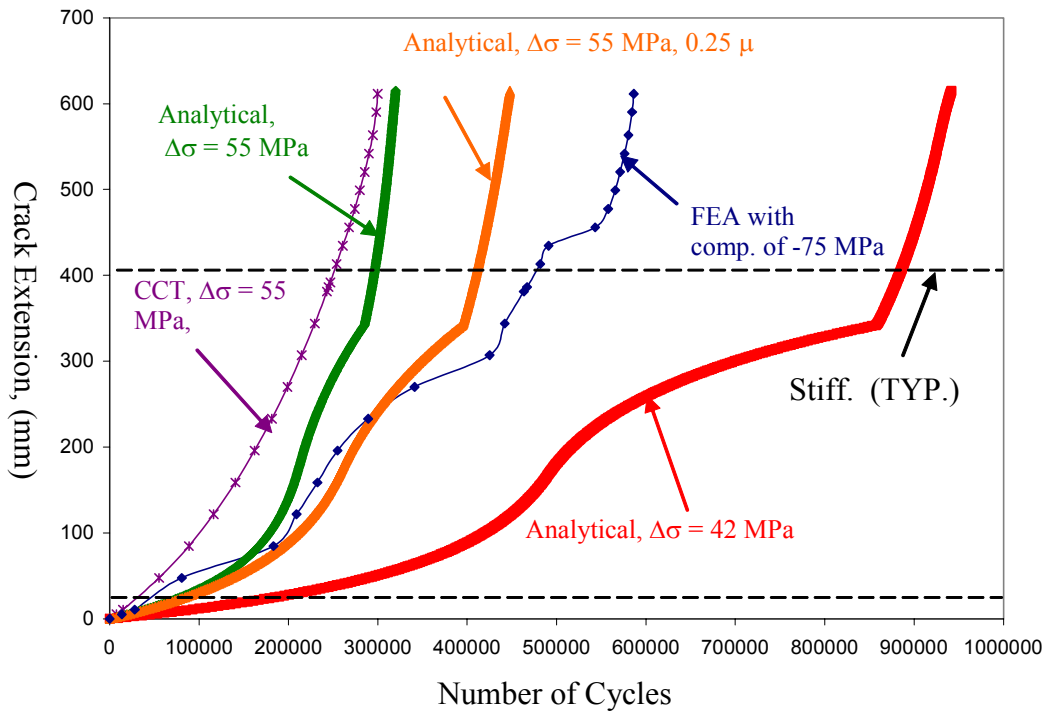

Figure 9-3 Comparison of finite-element results with 75 MPa compressive residual stress between stiffeners to Analytical Model with several applied stress range

With the analytical model, the relative magnitude of several different effects can be determined. Figure 9-4 shows the result of the analytical model corrected for shear lag compared to equivalent analyses with no restraint effect and no residual stress effect. It can be seen that both effects are about equally important. The case with no restraint effect tracks the CCT result until the residual stress kicks in at crack extension of about

200 mm.   Both cases with restraint have a delay in the crack propagation at the outset but then eventually becoming more or less parallel with the CCT result. Then the case with restraint and residual stresses begins another delay due to residual stress.
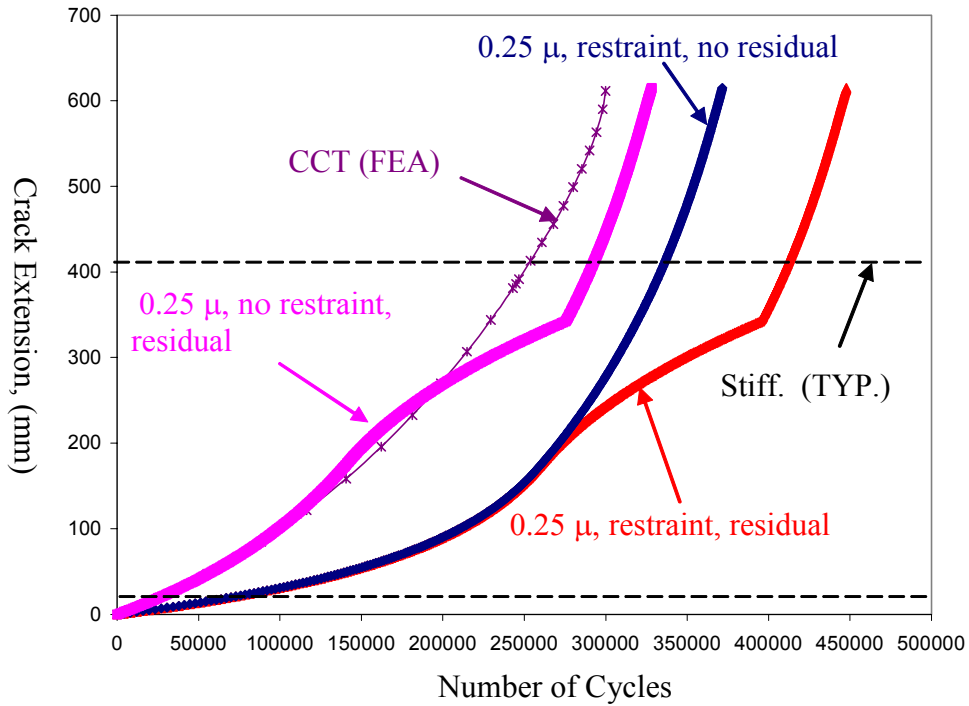

Figure 9-4 Comparison of finite-element results with 75 MPa compressive residual stress between stiffeners to Analytical Model with several applied stress range

SHIP STRUCTURE COMMITTEE PARTNERS AND LIAISON MEMBERS

PARTNERS

The Society of Naval Architects and Marine Engineers

Mr. Joe Cuneo
President,
Society of Naval Architects and Marine Engineers

Dr. John Daidola
Chairman,
SNAME Technical & Research Steering
Committee

The Gulf Coast Region Maritime Technology Center

Dr. John Crisp
Executive Director,
Gulf Coast Maritime Technology Center

Dr. Bill Vorus
Site Director,
Gulf Coast Maritime Technology Center

LIAISON MEMBERS

American Iron and Steel Institute	Mr. Alexander Wilson
American Society for Testing & Materials	Captain Charles Piersall (Ret.)
American Society of Naval Engineers	Captain Dennis K. Kruse (USN Ret.)
American Welding Society	Mr. Richard Frank
Bethlehem Steel Corporation	Dr. Harold Reemsnyder
Canada Center for Minerals & Energy Technology	Dr. William R. Tyson
Colorado School of Mines	Dr. Stephen Liu
Edison Welding Institute	Mr. Dave Edmonds
International Maritime Organization	Mr. Tom Allen
International Ship and Offshore Structure Congress	Dr. Alaa Mansour
INTERTANKO	Mr. Dragos Rauta
Massachusetts Institute of Technology	Mr. Dave Burke / Captain Chip McCord
Memorial University of Newfoundland	Dr. M. R. Haddara
National Cargo Bureau	Captain Jim McNamara
Office of Naval Research	Dr. Yapa Rajapaksie
Oil Companies International Maritime Forum	Mr. Phillip Murphy
Tanker Structure Cooperative Forum	Mr. Rong Huang
Technical University of Nova Scotia	Dr. C. Hsiung
United States Coast Guard Academy	Commander Kurt Colella
United States Merchant Marine Academy	Dr. C. B. Kim
United States Naval Academy	Dr. Ramswar Bhattacharyya
University of British Columbia	Dr. S. Calisal
University of California Berkeley	Dr. Robert Bea
University of Houston - Composites Eng & Appl.	Dr. Jerry Williams
University of Maryland	Dr. Bilal Ayyub
University of Michigan	Dr. Michael Bernitsas
University of Waterloo	Dr. J. Roorda
Virginia Polytechnic and State Institute	Dr. Alan Brown
Webb Institute	Dr. Kirsi Tikka
Welding Research Council	Dr. Martin Prager
Worchester Polytechnic Institute	Dr. Nick Dembsey
World Maritime Consulting, INC	VADM Gene Henn, USCG Ret.

RECENT SHIP STRUCTURE COMMITTEE PUBLICATIONS

Ship Structure Committee Publications on the Web - All reports from SSC 392 and forward are available to be downloaded from the Ship Structure Committee Web Site at URL:
http://www.shipstructure.org
SSC 391 and below are available on the SSC CD-ROM Library. Visit the National Technical Information Service (NTIS) Web Site for ordering information at URL:
http://www.ntis.gov/fcpc/cpn7833.htm

SSC Report Number   Report Bibliography

SSC 434	**Predicting Motion and Structural Loads in Stranded Ships Phase 1** A.J. Brown, M. Simbulan, J. McQuillan, M. Gutierrez 2004
SSC 433	**Interactive Buckling Testing of Stiffened Steel Plate Panels** Q. Chen, R.S. Hanson, G.Y. Grondin 2004
SSC 432	**Adaptation of Commercial Structural Criteria to Military Needs** R.Vara, C.M. Potter, R.A. Sielski, J.P. Sikora, L.R. Hill, J.C. Adamchak, D.P. Kihl, J. Hebert, R.I. Basu, L. Ferreiro, J. Watts, P.D. Herrington 2003
SSC 431	**Retention of Weld Metal Properties and Prevention of Hydrogen Cracking** R.J. Wong 2003
SSC 430	**Fracture Toughness of a Ship Structure** A.Dinovitzer, N. Pussegoda, 2003
SSC 429	**Rapid Stress Intensity Factor Solution Estimation for Ship Structures Applications** L. Blair Carroll, S. Tiku, A.S. Dinovitzer 2003
SSC 428	**In-Service Non-Destructive Evaluation of Fatigue and Fracture Properties for Ship Structure** S. Tiku 2003
SSC 427	**Life Expectancy Assessment of Ship Structures** A. Dinovitzer 2003
SSC 426	**Post Yield Stability of Framing** J. DesRochers, C. Pothier, E. Crocker 2003
SSC 425	**Fatigue Strength and Adequacy of Weld Repairs** R.J. Dexter, R.J. Fitzpatrick, D.L. St. Peters 2003
SSC 424	**Evaluation of Accidental Oil Spills from Bunker Tanks (Phase I)** T. McAllister, C. Rekart, K. Michel 2003
SSC 423	**Green Water Loading on Ship Deck Structures** M. Meinhold, D. Liut, K. Weems, T. Treakle, Woe-Min Lin 2003